Published for SISSA by Springer

Received: April 27, 2017
Revised: June 29, 2017
Accepted: July 25, 2017
Published: August 9, 2017

Resonances and CP violation in B_s^0 and $\overline{B}_s^0 \to J/\psi K^+K^-$ decays in the mass region above the $\phi(1020)$

The LHCb collaboration

E-mail: liming.zhang@cern.ch

Abstract: The decays of B_s^0 and $\overline{B}_s^0$ mesons into the $J/\psi K^+K^-$ final state are studied in the K^+K^- mass region above the $\phi(1020)$ meson in order to determine the resonant substructure and measure the CP-violating phase, ϕ_s, the decay width, Γ_s, and the width difference between light and heavy mass eigenstates, $\Delta\Gamma_s$. A decay-time dependent amplitude analysis is employed. The data sample corresponds to an integrated luminosity of $3\,\text{fb}^{-1}$ produced in 7 and 8 TeV pp collisions at the LHC, collected by the LHCb experiment. The measurement determines $\phi_s = 119 \pm 107 \pm 34\,\text{mrad}$. A combination with previous LHCb measurements using similar decays into the $J/\psi\pi^+\pi^-$ and $J/\psi\phi(1020)$ final states gives $\phi_s = 1 \pm 37\,\text{mrad}$, consistent with the Standard Model prediction.

Keywords: B physics, CP violation, Spectroscopy, Hadron-Hadron scattering (experiments)

ArXiv ePrint: 1704.08217

https://doi.org/10.1007/JHEP08(2017)037

JHEP08(2017)037

Contents

1 Introduction

Measurements of *CP* violation through the interference of B_s^0 mixing and decay amplitudes are particularly sensitive to the presence of unseen particles or forces. The Standard Model (SM) prediction of the *CP*-violating phase in quark-level $b \to c\bar{c}s$ transitions is very small, $\phi_s^{\rm SM} \equiv -2\arg\left(-\frac{V_{ts}V_{tb}^*}{V_{cs}V_{cb}^*}\right) = -36.5^{+1.3}_{-1.2}$ mrad [1]. Although subleading corrections from penguin amplitudes are ignored in this estimate, the interpretation of the current measurements is not affected, since those subleading terms are known to be small [2–4] compared to the experimental precision. Initial measurements of ϕ_s were performed at the Tevatron [5, 6], followed by LHCb measurements using both B_s^0 and $\overline{B}{}_s^0$ decays[1] into $J/\psi\pi^+\pi^-$ and $J/\psi K^+K^-$, with K^+K^- invariant masses[2] $m_{KK} < 1.05\,\text{GeV}$, from $3\,\text{fb}^{-1}$ of integrated luminosity. The measurements were found to be consistent with the SM value [7, 8], as are more recent and somewhat less accurate results from the CMS [9] and

[1] Whenever a flavour-specific decay is mentioned it also implies use of the charge-conjugate decay except when dealing with *CP*-violating quantities or other explicitly mentioned cases.

[2] Natural units are used where $\hbar$=c=1.

JHEP08(2017)037

ATLAS [10] collaborations using $J/\psi\,\phi(1020)$ final states.[3] The average of all of the above mentioned measurements is $\phi_s = -30 \pm 33\,\text{mrad}$ [13].[4]

Previously, using a data sample corresponding to $1\,\text{fb}^{-1}$ integrated luminosity, the LHCb collaboration studied the resonant structures in the $B_s^0 \to J/\psi\,K^+K^-$ decay [14] revealing a rich resonance spectrum in the K^+K^- mass distribution. In addition to the $\phi(1020)$ meson, there are significant contributions from the $f_2'(1525)$ resonance [15] and nonresonant S-wave, which are large enough to allow further studies of *CP* violation. This paper presents the first measurement of ϕ_s using $B_s^0 \to J/\psi\,K^+K^-$ decays, where $J/\psi \to \mu^+\mu^-$ with m_{KK} above the $\phi(1020)$ region, using data corresponding to an integrated luminosity of $3\,\text{fb}^{-1}$, obtained from pp collisions at the LHC. One third of the data was collected at a centre-of-mass energy of 7 TeV, and the remainder at 8 TeV. An amplitude analysis as a function of the B_s^0 proper decay time [16] is performed to determine the *CP*-violating phase ϕ_s, by measuring simultaneously the *CP*-even and *CP*-odd decay amplitudes for each contributing resonance (and nonresonant S-wave), allowing the improvement of the ϕ_s accuracy and, in addition, further studies of the resonance composition in the decay.

These $B_s^0 \to J/\psi\,K^+K^-$ decays are separated into two K^+K^- mass intervals. Those with $m_{KK} < 1.05\,\text{GeV}$ are called low-mass and correspond to the region of the $\phi(1020)$ resonance, while those with $m_{KK} > 1.05\,\text{GeV}$ are called high-mass. The high-mass region has not been analyzed for *CP* violation before, allowing the measurement of *CP* violation in several decay modes, including a vector-tensor final state, $J/\psi\,f_2'(1525)$. In the SM the phase ϕ_s is expected to be the same in all such modes. One important difference from the previous low-mass analysis [7] is that modelling of the m_{KK} distribution is included to distinguish different resonance and nonresonance contributions. In the previous low mass *CP*-violation analysis only the $\phi(1020)$ resonance and an S-wave amplitude were considered. This analysis follows very closely the analyses of *CP* violation in $B_s^0 \to J/\psi\,\pi^+\pi^-$ decays [8] and in $B^0 \to J/\psi\,\pi^+\pi^-$ decays [3], and only significant changes with respect to those measurements are described in this paper. The analysis strategy is to fit the *CP*-even and *CP*-odd components in the decay width probability density functions that describe the interfering amplitudes in the particle and antiparticle decays. These fits are done as functions of the B_s^0 proper decay time and in a four-dimensional phase space including the three helicity angles characterizing the decay and m_{KK}. Flavour tagging, described below, allows us to distinguish between initial B_s^0 and $\overline{B}_s^0$ states.

This paper is organized as follows. Section 2 describes the B_s^0 proper-time dependent decay widths. Section 3 gives a description of the detector and the associated simulations. Section 4 contains the event selection procedure and the extracted signal yields. Section 5 shows the measurement of the proper-time resolution and efficiencies for the final state in the four-dimensional phase space. Section 6 summarizes the identification of the initial flavour of the state, a process called flavour tagging. Section 7 gives the masses and widths of resonant states that decay into K^+K^-, and the description of a model-independent S-wave parameterization. Section 8 describes the unbinned likelihood fit procedure used

[3]The final states $D_s^+D_s^-$ [11] and $\psi(2S)\phi(1020)$ [12] are also used by LHCb, but the precisions are not comparable due to lower statistics.

[4]See also updated results and plots available at http://www.slac.stanford.edu/xorg/hfag/.

JHEP08(2017)037

to determine the physics parameters, and presents the results of the fit, while section 9 discusses the systematic uncertainties. Finally, the results are summarized and combined with other measurements in section 10.

2 Decay rates for B_s^0 and $\overline{B}_s^0 \to J/\psi K^+K^-$

The total decay amplitude for a B_s^0 ($\overline{B}_s^0$) meson at decay time equal to zero is taken to be the sum over individual K^+K^- resonant transversity amplitudes [17], and one nonresonant amplitude, with each component labelled as A_i ($\overline{A}_i$). Because of the spin-1 J/ψ in the final state, the three possible polarizations of the J/ψ generate longitudinal (0), parallel ($\parallel$) and perpendicular ($\perp$) transversity amplitudes. When the K^+K^- forms a spin-0 state the final system only has a longitudinal component. Each of these amplitudes is a pure CP eigenstate. By introducing the parameter $\lambda_i \equiv \frac{q}{p}\frac{\overline{A}_i}{A_i}$, relating CP violation in the interference between mixing and decay associated with the state i, the total amplitudes $\mathcal{A}$ and $\overline{\mathcal{A}}$ can be expressed as the sums of the individual B_s^0 amplitudes, $\mathcal{A} = \sum A_i$ and $\overline{\mathcal{A}} = \sum \frac{q}{p}\overline{A}_i = \sum \lambda_i A_i = \sum \eta_i |\lambda_i| e^{-i\phi_s^i} A_i$. The quantities q and p relate the mass to the flavour eigenstates [18]. For each transversity state i the CP-violating phase $\phi_s^i \equiv -\arg(\eta_i\lambda_i)$ [19], with η_i being the CP eigenvalue of the state. Assuming that any possible CP violation in the decay is the same for all amplitudes, then $\lambda \equiv \eta_i\lambda_i$ and $\phi_s \equiv -\arg(\lambda)$ are common. The decay rates into the $J/\psi K^+K^-$ final state are[5]

$$\Gamma(t) \propto e^{-\Gamma_s t}\left\{\frac{|\mathcal{A}|^2+|\overline{\mathcal{A}}|^2}{2}\cosh\frac{\Delta\Gamma_s t}{2} + \frac{|\mathcal{A}|^2-|\overline{\mathcal{A}}|^2}{2}\cos(\Delta m_s t) - \mathcal{R}e(\mathcal{A}^*\overline{\mathcal{A}})\sinh\frac{\Delta\Gamma_s t}{2} - \mathcal{I}m(\mathcal{A}^*\overline{\mathcal{A}})\sin(\Delta m_s t)\right\}, \tag{2.1}$$

$$\overline{\Gamma}(t) \propto e^{-\Gamma_s t}\left\{\frac{|\mathcal{A}|^2+|\overline{\mathcal{A}}|^2}{2}\cosh\frac{\Delta\Gamma_s t}{2} - \frac{|\mathcal{A}|^2-|\overline{\mathcal{A}}|^2}{2}\cos(\Delta m_s t) - \mathcal{R}e(\mathcal{A}^*\overline{\mathcal{A}})\sinh\frac{\Delta\Gamma_s t}{2} + \mathcal{I}m(\mathcal{A}^*\overline{\mathcal{A}})\sin(\Delta m_s t)\right\}, \tag{2.2}$$

where $\Delta\Gamma_s \equiv \Gamma_{\rm L} - \Gamma_{\rm H}$ is the decay width difference between the light and the heavy mass eigenstates, $\Delta m_s \equiv m_{\rm H} - m_{\rm L}$ is the mass difference, and $\Gamma_s \equiv (\Gamma_{\rm L}+\Gamma_{\rm H})/2$ is the average width. The sensitivity to the phase ϕ_s is driven by the terms containing $\mathcal{A}^*\overline{\mathcal{A}}$.

For J/ψ decays to $\mu^+\mu^-$ final states, these amplitudes are themselves functions of four variables: the K^+K^- invariant mass m_{KK}, and three angular variables $\Omega \equiv (\cos\theta_{KK}, \cos\theta_{J/\psi}, \chi)$, defined in the helicity basis. These consist of the angle θ_{KK} between the K^+ direction in the K^+K^- rest frame with respect to the K^+K^- direction in the B_s^0 rest frame, the angle $\theta_{J/\psi}$ between the μ^+ direction in the J/ψ rest frame with respect to the J/ψ direction in the B_s^0 rest frame, and the angle χ between the J/ψ and K^+K^- decay planes in the B_s^0 rest frame [16, 19]. These angles are shown pictorially in figure 1. These definitions are the same for B_s^0 and $\overline{B}_s^0$, namely, using μ^+ and K^+ to define the angles for both B_s^0 and $\overline{B}_s^0$ decays. The explicit forms of $|\mathcal{A}(m_{KK},\Omega)|^2$, $|\overline{\mathcal{A}}(m_{KK},\Omega)|^2$, and $\mathcal{A}^*(m_{KK},\Omega)\overline{\mathcal{A}}(m_{KK},\Omega)$ in eqs. (2.1) and (2.2) are given in ref. [16].

[5] $|p/q| = 1$ is used. The latest LHCb measurement determined $|p/q|^2 = 1.0039 \pm 0.0033$ [20].

JHEP08(2017)037

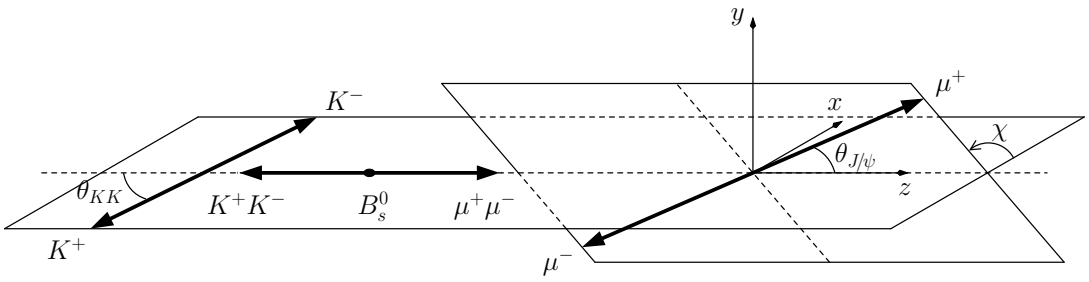

Figure 1. Definition of the helicity angles.

3 Detector and simulation

The LHCb detector [21, 22] is a single-arm forward spectrometer covering the pseudorapidity range $2 < \eta < 5$, designed for the study of particles containing b or c quarks. The detector includes a high-precision tracking system consisting of a silicon-strip vertex detector surrounding the pp interaction region, a large-area silicon-strip detector located upstream of a dipole magnet with a bending power of about 4 Tm, and three stations of silicon-strip detectors and straw drift tubes placed downstream of the magnet. The tracking system provides a measurement of momentum, p, of charged particles with a relative uncertainty that varies from 0.5% at low momentum to 1.0% at 200 GeV. The primary vertex (PV) is constructed from reconstructed tracks that arise from a common origin [23]. The minimum distance of a track to a PV, the impact parameter (IP), is measured with a resolution of $(15 + 29/p_{\mathrm{T}})$ μm, where p_{T} is the component of the momentum transverse to the beam, in GeV. Different types of charged hadrons are distinguished using information from two ring-imaging Cherenkov (RICH) detectors. Photons, electrons and hadrons are identified by a calorimeter system consisting of scintillating-pad and preshower detectors, an electromagnetic calorimeter and a hadronic calorimeter. Muons are identified by a system composed of alternating layers of iron and multiwire proportional chambers.

The online event selection is performed by a trigger, which consists of a hardware stage, based on information from the calorimeter and muon systems, followed by a software stage, which applies a full event reconstruction. The software trigger is composed of two stages, the first of which performs a partial reconstruction and requires either a pair of well-reconstructed, oppositely charged muons having an invariant mass above 2.7 GeV, or a single well-reconstructed muon with high p_{T} and large IP. The second stage applies a full event reconstruction and for this analysis requires two opposite-sign muons to form a good-quality vertex that is well separated from all of the PVs, and to have an invariant mass within ±120 MeV of the known J/ψ mass [24].

In the simulation, pp collisions are generated using Pythia 8 [25, 26]. Decays of hadronic particles are described by EvtGen [27], in which final-state radiation is generated using Photos [28]. The interaction of the generated particles with the detector, and its response, are implemented using the Geant4 toolkit [29, 30] as described in ref. [31]. The simulation covers the full K^+K^- mass range.

JHEP08(2017)037

4 Event selection and signal yield extraction

A B_s^0 candidate is reconstructed by combining a $J/\psi \to \mu^+\mu^-$ candidate with two kaons of opposite charge. The offline selection uses a loose preselection, followed by a multivariate classifier based on a Gradient Boosted Decision Tree (BDTG) [32].

In the preselection, the J/ψ candidates are formed from two oppositely charged particles with $p_{\rm T}$ greater than 550 MeV, identified as muons and consistent with originating from a common vertex but inconsistent with originating from any PV. The invariant mass of the $\mu^+\mu^-$ pair is required to be within $[-48, +43]$ MeV of the known J/ψ mass [24], corresponding to a window of about ± 3 times the mass resolution. The asymmetry in the cut values is due to the radiative tail. The two muons are subsequently kinematically constrained to the known J/ψ mass. Kaon candidates are required to be positively identified in the RICH detectors, to have $p_{\rm T}$ greater than 250 MeV, and the scalar sum of the two transverse momenta, $p_{\rm T}(K^+) + p_{\rm T}(K^-)$, must be larger than 900 MeV.

The four tracks from a B_s^0 candidate decay must originate from a common vertex with a good fit χ^2 and have a decay time greater than 0.3 ps. Each B_s^0 candidate is assigned to a PV for which it has the smallest $\chi^2_{\rm IP}$, defined as the difference in the χ^2 of the vertex fit for a given PV reconstructed with and without the considered particle. The angle between the momentum vector of the B_s^0 decay candidates and the vector formed from the positions of the PV and the decay vertex (pointing angle) is required to be less than 2.5°.

Events are filtered with a BDTG to further suppress the combinatorial background. The BDTG uses six variables: $p_{\rm T}(K^+) + p_{\rm T}(K^-)$; the vertex-fit χ^2, pointing angle, $\chi^2_{\rm IP}$, and $p_{\rm T}$ of the B_s^0 candidates; and the smaller of the DLL$(\mu - \pi)$ for the two muons, where DLL$(\mu - \pi)$ is the difference in the logarithms of the likelihood values from the particle identification systems [33] for the muon and pion hypotheses. The BDTG is trained on a simulated sample of 0.7 million reconstructed $B_s^0 \to J/\psi K^+K^-$ signal events, with the final-state particles generated uniformly in phase space assuming unpolarized $J/\psi \to \mu^+\mu^-$ decays, and a background data sample from the sideband $5516 < m(J/\psi K^+K^-) < 5616$ MeV. Separate samples are used to train and test the BDTG. The BDTG and particle identification (PID) requirements for the kaons are chosen to maximize the signal significance multiplied by the square root of the purity, $S/\sqrt{S+B} \times \sqrt{S/(S+B)}$, for candidates with $m_{KK} > 1.05$ GeV, where S and B are the numbers of signal and background candidate combinations, respectively. This figure of merit optimizes the total uncertainty including both statistical and background systematic errors.

In addition to the expected combinatorial background, studies of the data in sidebands of the $m(J/\psi K^+K^-)$ spectrum show contributions from approximately 8700 (430) $\overline{B}^0 \to J/\psi K^-\pi^+$ and 10 700 (800) $\Lambda_b^0 \to J/\psi pK^-$ decays at m_{KK} greater (less) than 1.05 GeV, where the π^+ in the former or p in the latter is misidentified as a K^+. In order to avoid dealing with correlations between the angular variables and $m(J/\psi K^+K^-)$, the contributions from these reflection backgrounds are statistically subtracted by adding to the data simulated events of these decays with negative weights. These weights are chosen so that the distributions of the relevant variables used in the overall fit (see below) describe the background distributions both in normalization and shapes. The simulation uses amplitude models derived from data for $\overline{B}^0 \to J/\psi K^-\pi^+$ [34] and $\Lambda_b^0 \to J/\psi pK^-$ decays [35].

JHEP08(2017)037

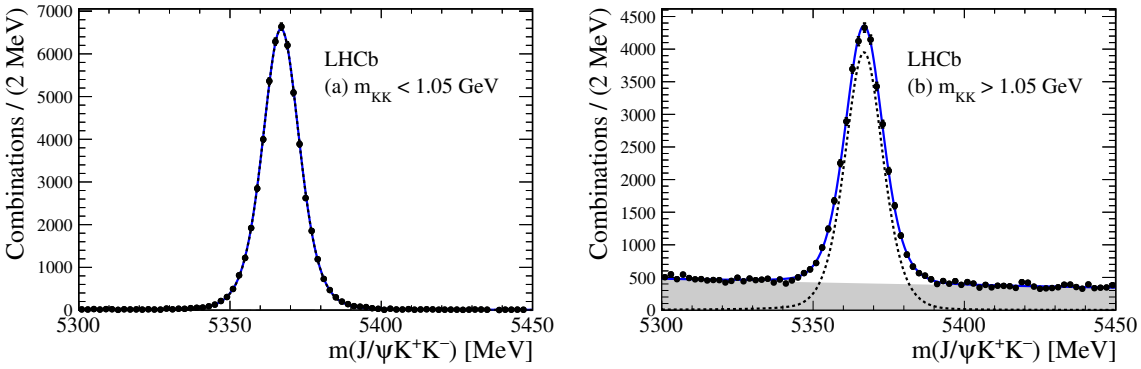

Figure 2. Fits to invariant mass distributions of $J/\psi K^+K^-$ combinations after subtraction of the two reflection backgrounds for (a) $m_{KK} < 1.05\,\text{GeV}$ and (b) $m_{KK} > 1.05\,\text{GeV}$. Total fits are shown by solid (blue) lines, the signal by dashed (black) lines, and the combinatorial background by darkened regions. Note that the combinatorial background in (a) is too small to be easily visible.

The invariant mass of the selected $J/\psi K^+K^-$ combinations, separated into samples for m_{KK} below or above 1.05 GeV, are shown in figure 2, where the expected reflection backgrounds are subtracted using simulation. The combinatorial background is modelled with an exponential function and the B_s^0 signal shape is parameterized by a double-sided Hypatia function [36], where the signal radiative tail parameters are fixed to values obtained from simulation. In total, $53\,440 \pm 240$ and $33\,200 \pm 240$ signal candidates are found for the low and high m_{KK} intervals, respectively. Figure 3 shows the Dalitz plot distribution of $m^2_{K^+K^-}$ versus $m^2_{J/\psi K^+}$ for $B_s^0 \to J/\psi K^+K^-$ candidates within $\pm 15\,\text{MeV}$ of the B_s^0 mass peak. Clear resonant contributions from $\phi(1020)$ and $f_2'(1525)$ mesons are seen, but no exotic $J/\psi K^+$ resonance is observed.

5 Detector resolution and efficiency

The resolution on the decay time is determined with the same method as described in ref. [7] by using a large sample of prompt $J/\psi K^+K^-$ combinations produced directly in the pp interactions. These events are selected using $J/\psi \to \mu^+\mu^-$ decays via a prescaled trigger that does not impose any requirements on the separation of the J/ψ from the PV. The J/ψ candidates are combined with two oppositely charged tracks that are identified as kaons, using a similar selection as for the signal decay, without a decay-time requirement. The resolution function, $T(t - \hat{t}\,|\,\delta_t)$, where $\hat{t}$ is the true decay time, is a sum of three Gaussian functions with a common mean, and separate widths. To implement the resolution model each of the three widths are given by $S_i \cdot (\delta_t + \sigma_t^0)$, where S_i is scale factor for the ith Gaussian, δ_t is an estimated per-candidate decay-time error and σ_t^0 is a constant parameter. The parameters of the resolution model are determined by using a maximum likelihood fit to the unbinned decay time and δ_t distributions of the prompt $J/\psi K^+K^-$ combinations, using a δ function to represent the prompt component summed with two exponential functions for long-lived backgrounds; these are convolved with the resolution function. Taking into account the δ_t distribution of the B_s^0 signal, the average effective resolution is found to be 44.7 fs.

JHEP08(2017)037

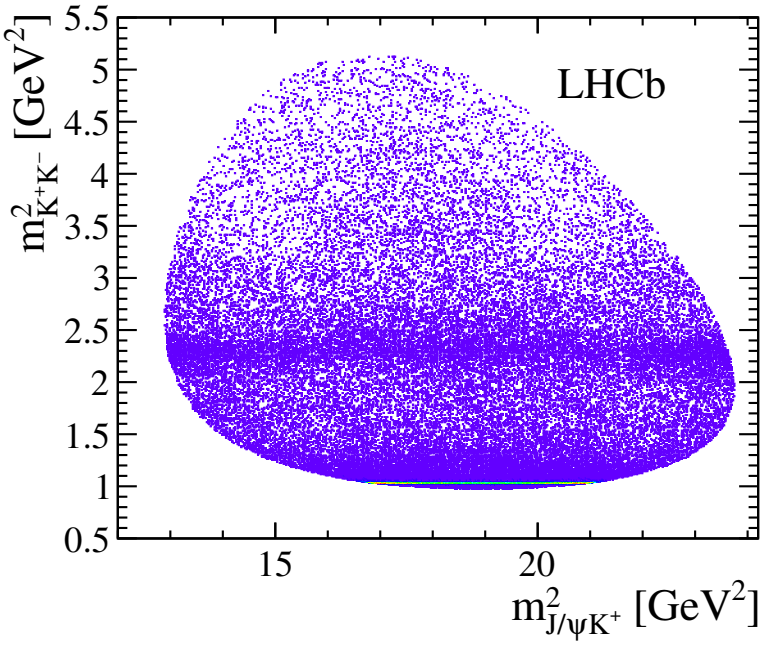

Figure 3. Invariant mass squared of K^+K^- versus $J/\psi K^+$ for $B_s^0 \to J/\psi K^+K^-$ candidates within ± 15 MeV of the B_s^0 mass peak. The high intensity $\phi(1020)$ resonance band is shown with a line (light green).

The reconstruction efficiency is not constant as a function of decay time due to displacement requirements made on the J/ψ candidates in the trigger and offline selections. The efficiency is determined using the control channel $B^0 \to J/\psi K^*(892)^0$, with $K^*(892)^0 \to K^+\pi^-$, which is known to have a purely exponential decay-time distribution with $\tau_{B^0} = 1.520 \pm 0.004$ ps [24]. The selection efficiency is calculated as

$$\varepsilon^{B_s^0}_{\rm data}(t) = \varepsilon^{B^0}_{\rm data}(t) \times \frac{\varepsilon^{B_s^0}_{\rm sim}(t)}{\varepsilon^{B^0}_{\rm sim}(t)}, \tag{5.1}$$

where $\varepsilon^{B^0}_{\rm data}(t)$ is the efficiency of the control channel and $\varepsilon^{B_s^0}_{\rm sim}(t)/\varepsilon^{B^0}_{\rm sim}(t)$ is the ratio of efficiencies of the simulated signal and control mode after the full trigger and selection chain has been applied. This correction accounts for the small differences in the kinematics between the signal and control mode. The details of the method are explained in ref. [8]. The decay-time efficiencies for the two m_{KK} intervals are shown in figure 4.

The efficiency as a function of the $B_s^0 \to J/\psi K^+K^-$ helicity angles and the K^+K^- invariant mass is not uniform due to the forward geometry of the LHCb detector and the requirements imposed on the final-state particle momenta. The four-dimensional efficiency, $\varepsilon(m_{KK}, \Omega)$, is determined using simulated events that are subjected to the same trigger and selection criteria as the data.

The efficiency is parameterized by

$$\epsilon(m_{KK}, \Omega) = \sum_{a,b,c,d} \epsilon^{abcd} \mathcal{P}_a(\cos\theta_{KK}) Y_{bc}(\theta_{J/\psi}, \chi) \mathcal{P}_d\left(2\frac{m_{KK} - m_{KK}^{\rm min}}{m_{KK}^{\rm max} - m_{KK}^{\rm min}} - 1\right), \tag{5.2}$$

JHEP08(2017)037

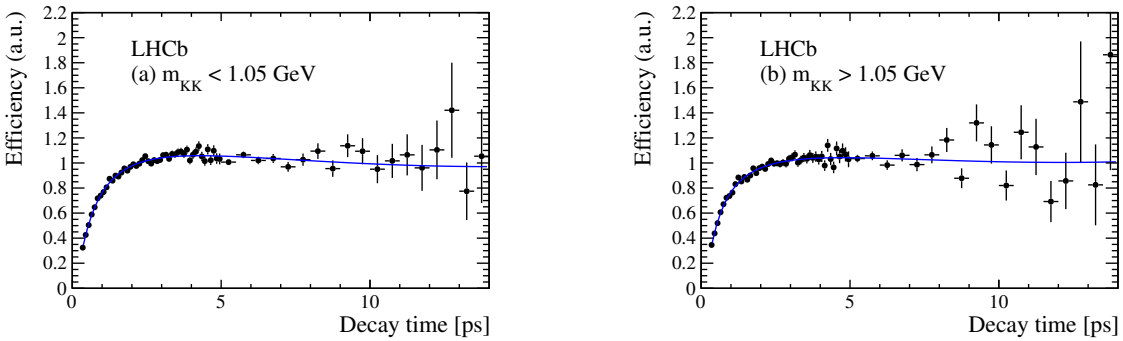

Figure 4. Scaled decay-time efficiency $\varepsilon^{B_s^0}_{\rm data}(t)$ in arbitrary units (a.u.) for (a) the $\phi(1020)$ region and (b) the high-mass region.

where $\mathcal{P}_a$ and $\mathcal{P}_d$ are Legendre polynomials, Y_{bc} are spherical harmonics, and $m^{\rm min}_{KK} = 2m_{K^+}$ and $m^{\rm max}_{KK} = m_{B^0_s} - m_{J/\psi}$ are the minimum and maximum allowed values for m_{KK}, respectively. The Y_{bc} are complex functions. To ensure that the efficiency function is real, we set $\epsilon^{abcd} = -\epsilon^{ab(-c)d}$. The values of ϵ^{abcd} are determined by summing over the fully simulated phase-space events

$$\epsilon^{abcd} = \frac{1}{\sum_i w_i}\sum_i w_i \frac{2a+1}{2}\frac{2d+1}{2}\mathcal{P}_a(\cos\theta_{KK,i})Y^*_{bc}(\theta_{J/\psi,i},\chi_i)\mathcal{P}_d\left(2\frac{m_{KK,i}-m^{\rm min}_{KK}}{m^{\rm max}_{KK}-m^{\rm min}_{KK}}-1\right)\frac{1}{g_i}, \tag{5.3}$$

where the weights w_i account for corrections of PID and tracking efficiencies, and $g_i = P^i_R P^i_B$ is the value of the phase-space probability density for event i with P_R being the momentum of either of the two hadrons in the dihadron rest frame and P_B the momentum of the J/ψ in the B^0_s rest frame. This approach allows the description of multidimensional correlations without assuming factorization. In practice, the sum is over a finite number of terms ($a \leq 10$, $b \leq 8$, $-2 \leq c \leq 2$, $d \leq 8$) and only coefficients with a statistical significance larger than three standard deviations (σ) from zero are retained. The number of events in the simulated signal sample is about 20 times of that observed in data. Since a symmetric K^+ and K^- efficiency is used, a and $b+c$ must be even numbers. Projections of the efficiency integrated over other variables are shown in figure 5. The modelling functions describe well the simulated data. Since $\chi^2_{\rm IP}$ is not used as a variable in the selection for the two hadrons, the efficiency is quite uniform over all the four variables varying only by about $\pm 10\%$. (A dedicated simulation of $J/\psi\,\phi(1020)$ decays is used to determine the efficiency in the region of $m_{KK} < 1.05\,\text{GeV}$, in order to have a large enough sample for an accurate determination.)

6 Flavour tagging

The B^0_s candidate flavour at production is determined using two independent classes of flavour-tagging algorithms, the opposite-side (OS) tagger [37] and the same-side kaon (SSK) tagger [38], which exploit specific features of the production of $b\bar{b}$ quark pairs in pp collisions, and their subsequent hadronisation. Each tagging algorithm provides a tag decision and

JHEP08(2017)037

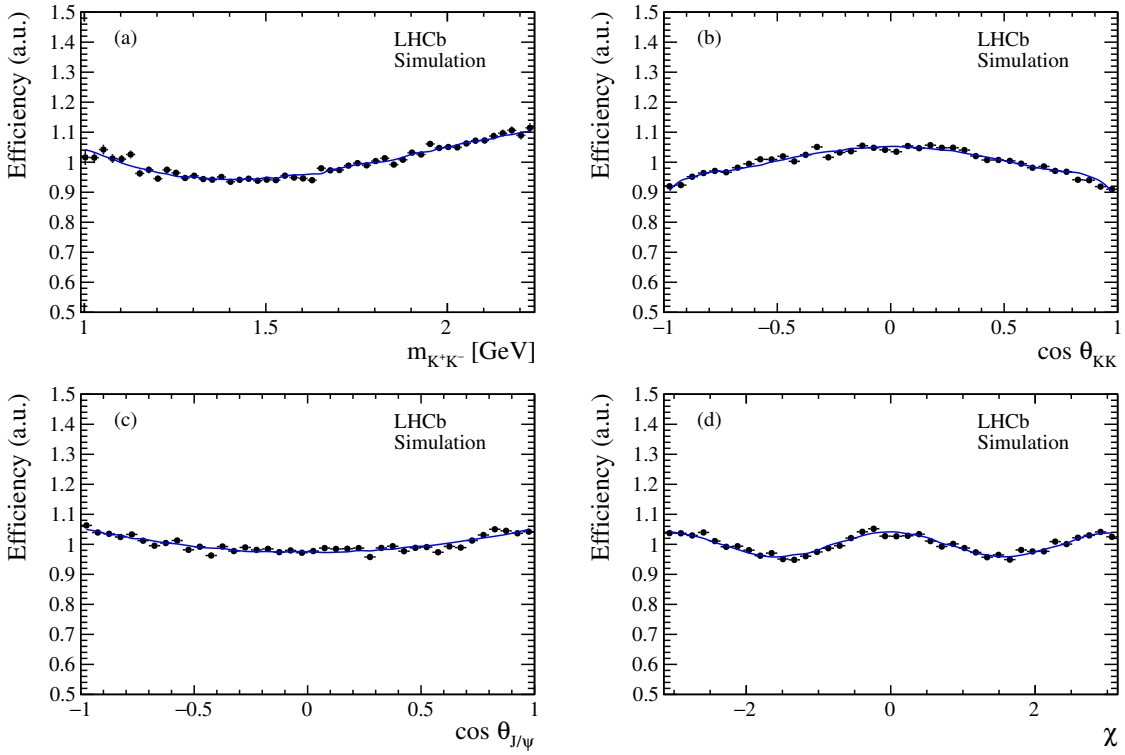

Figure 5. Efficiencies projected onto (a) m_{KK}, (b) $\cos\theta_{KK}$, (c) $\cos\theta_{J/\psi}$ and (d) χ in arbitrary units (a.u.), obtained from simulation of $B_s^0 \to J/\psi K^+K^-$ phase-space decays (points with error bars), while the curves show the parameterization from the efficiency model.

a mistag probability. The tag decision, $\mathfrak{q}$, is $+1$, -1, or 0, if the signal meson is tagged as B_s^0, $\overline{B}{}_s^0$, or is untagged, respectively. The fraction of candidates in the sample with a nonzero tagging decision gives the efficiency of the tagger, $\varepsilon_{\rm tag}$. The mistag probability, η, is estimated event by event, and represents the probability that the algorithm assigns a wrong tag decision to the candidate; it is calibrated using data samples of several flavour-specific B^0, B^+, B_s^0 and B_{s2}^{*0} [38] decays to obtain the corrected mistag probability, ω, for an initial B_s^0 meson, and separately obtain $\overline{\omega}$ for an initial $\overline{B}{}_s^0$ meson. A linear relationship between η and $(\overline{\omega})$ is used for the calibration. When candidates are tagged by both the OS and the SSK algorithms, a combined tag decision and a wrong-tag probability are given by the algorithm defined in ref. [37] and extended to include SSK tags. This combined algorithm is implemented in the overall fit. The effective tagging power is given by $\varepsilon_{\rm tag}\left\langle(1-2\omega)^2\right\rangle$ and for the combined taggers in the $B_s^0 \to J/\psi K^+K^-$ signal sample is $(3.82\pm0.13\pm0.12)\%$. Whenever two uncertainties are quoted in this paper, the first is statistical and the second is systematic.

7 Resonance contributions

The entire K^+K^- mass spectrum is fitted by including the resonance contributions previously found in the time-integrated amplitude analysis using $1\,\text{fb}^{-1}$ of integrated luminos-

JHEP08(2017)037

Resonance	Mass (MeV)	Width (MeV)	Source
$\phi(1020)$	1019.461 ± 0.019	4.266 ± 0.031	PDG [24]
$f_2(1270)$	1275.5 ± 0.8	$186.7^{+2.2}_{-2.5}$	PDG [24]
$f_2'(1525)$	Varied in fits		
$\phi(1680)$	1689 ± 12	211 ± 24	Belle [39]
$f_2(1750)$	1737 ± 9	151 ± 33	Belle [40]
$f_2(1950)$	1980 ± 14	297 ± 13	Belle [40]

Table 1. Breit-Wigner resonance parameters.

ity [14], except for the unconfirmed $f_2(1640)$ state. They are shown in table 1 and are described by Breit-Wigner amplitudes. The S-wave amplitude $\mathcal{S}(m_{KK}) = c(m_{KK}) + is(m_{KK})$ is described in a model-independent way, making no assumptions about its f_0 meson composition, or about the form of any S-wave nonresonant terms. Explicitly, two real parameters $c^k = c(m^k_{KK})$ and $s^k = s(m^k_{KK})$ are introduced to define the total S-wave amplitude at each of a set of invariant mass values $m_{KK} = m^k_{KK}$ $(k = 1, \ldots, N_s)$. Third-order spline interpolations are used to define $c(m_{KK})$ and $s(m_{KK})$ between these points of m^k_{KK}. The c^k and s^k values are treated as model-independent parameters, and are determined by a fit to the data. In total $N_s = 13$ knots are chosen at $m_{KK} = (1.01, 1.03, 1.05, 1.10, 1.40, 1.50, 1.65, 1.70, 1.75, 1.80, 1.90, 2.1, 2.269)$ GeV. The S-wave amplitude is proportional to momentum P_B [16]; at the last point since $P_B = 0$, the amplitude is zero [16].

To describe the m_{KK} dependence for each resonance R, the formula of eq. (18) in ref. [16] is modified by changing $\left(\frac{P_R}{m_{KK}}\right)^{L_R}$ to $\left(\frac{P_R}{m_0}\right)^{L_R}$, where P_R is the momentum of either of the two hadrons in the dihadron rest frame, m_0 is the mass of resonance R, and L_R the orbital angular momentum in the K^+K^- decay, and thus corresponds to the resonance's spin. This change modifies the lineshape of resonances with spin greater than zero. The original formula followed the convention from the Belle collaboration [41] and was used in two LHCb publications [3, 14], while the new one follows the convention of PDG/EvtGen, and was used in analyzing $\Lambda_b^0 \to J/\psi p K^-$ decays [35].

8 Maximum likelihood fit

The physics parameters are determined from a weighted maximum likelihood fit of a signal-only probability density function (PDF) to the five-dimensional distributions of B_s^0 and $\overline{B}_s^0$ decay time, m_{KK} and helicity angles. The negative log-likelihood function to be minimized is given by

$$-\ln \mathcal{L} = -\alpha \sum_i W_i \ln(\mathcal{P}\mathcal{D}\mathcal{F}), \tag{8.1}$$

where i runs over all event candidates, W_i is the *sWeight* computed using $m(J/\psi K^+K^-)$ as the discriminating variable [42, 43] and the factor $\alpha \equiv \sum_i W_i / \sum_i W_i^2$ is a constant factor accounting for the effect of the background subtraction on the statistical uncertainty. The

JHEP08(2017)037

Parameter	Value
Γ_s [ps^{-1}]	$0.650 \pm 0.006 \pm 0.004$
$\Delta\Gamma_s$ [ps^{-1}]	$0.066 \pm 0.018 \pm 0.010$
ϕ_s [mrad]	$119 \pm 107 \pm 34$
$\lvert\lambda\rvert$	$0.994 \pm 0.018 \pm 0.006$

Table 2. Fit results for the B_s^0 decay observables in the high m_{KK} region.

sWeights are determined by separate fits in four $|\cos\theta_{J/\psi}|$ bins for the event candidates. The PDF is given by $\mathcal{PDF} = \mathcal{F}/\int \mathcal{F} \mathrm{d}t\, \mathrm{d}m_{KK}\, \mathrm{d}\Omega$, where $\mathcal{F}$ is

$$\mathcal{F}(t, m_{KK}, \Omega, \mathfrak{q} \,|\, \eta, \delta_t) = \left[\mathcal{R}(\hat{t}, m_{KK}, \Omega, \mathfrak{q} \,|\, \eta) \otimes T(t - \hat{t} \,|\, \delta_t)\right] \cdot \varepsilon^{B_s^0}_{\mathrm{data}}(t) \cdot \varepsilon(m_{KK}, \Omega), \quad (8.2)$$

with

$$\mathcal{R}(\hat{t}, m_{KK}, \Omega, \mathfrak{q} \,|\, \eta) = \frac{1}{1 + |\mathfrak{q}|}\Bigg[[1 + \mathfrak{q}\,(1 - 2\omega(\eta))]\,\Gamma(\hat{t}, m_{KK}, \Omega) + [1 - \mathfrak{q}\,(1 - 2\bar{\omega}(\eta))]\,\frac{1 + A_{\mathrm{P}}}{1 - A_{\mathrm{P}}}\bar{\Gamma}(\hat{t}, m_{KK}, \Omega)\Bigg], \quad (8.3)$$

where $\hat{t}$ is the true decay time, $\overset{(-)}{\Gamma}$ is defined in eqs. (2.1) and (2.2), and $A_{\mathrm{P}} = (1.09 \pm 2.69)\%$ is the LHCb measured production asymmetry of B_s^0 and $\overline{B}{}_s^0$ mesons [44, 45].

To obtain a measurement that is independent of the previous publication that used mainly $J/\psi\,\phi(1020)$ decays [7], two different sets of fit parameters $(\phi_s, |\lambda|, \Gamma_s, \Delta\Gamma_s)^{\mathrm{L,H}}$ are used to account for the low (L) and high (H) m_{KK} regions. Simulated pseudoexperiments show that this configuration removes the correlation for these parameters between the two regions. A simultaneous fit to the two samples is performed by constructing the log-likelihood as the sum of that computed from the L and H events. The shared parameters are all the resonance amplitudes and phases, and Δm_s, which is freely varied in the fit. In the nominal fit configuration, *CP* violation is assumed to be the same for all the transversity states. In total 69 free parameters are used in the nominal fit.

The B_s^0 decay observables resulting from the fit for the high m_{KK} region are listed in table 2. The measurements for these parameters and Δm_s in the $\phi(1020)$ region are consistent with the reported values in ref. [7] within 1.4σ, taking into account the overlap between the two samples used. In addition, good agreement is also found for the S-wave phase. The fit gives $\Delta m_s = 17.783 \pm 0.049\,(\mathrm{stat})\,\mathrm{ps}^{-1}$ from the full m_{KK} region, which is consistent with the most precise measurement $17.768 \pm 0.023 \pm 0.006\,\mathrm{ps}^{-1}$ from LHCb in $B_s^0 \to D_s^-\pi^+$ decays [46]. The value of $|\lambda|$ is consistent with unity, thus giving no indication of any direct *CP* violation in the decay amplitude.

While a complete description of the $\overline{B}{}_s^0 \to J/\psi\,K^+K^-$ decay is given in terms of the fitted amplitudes and phases, knowledge of the contribution of each component can be summarized by the fit fraction, FF_i, defined as the integral of the squared amplitude of each resonance over the phase space divided by the integral of the entire signal function

JHEP08(2017)037

Component	Fit fraction (%)	Transversity fraction (%)		
		0	$\parallel$	$\perp$
$\phi(1020)$	$70.5 \pm 0.6 \pm 1.2$	50.9 ± 0.4	23.1 ± 0.5	26.0 ± 0.6
$f_2(1270)$	$1.6 \pm 0.3 \pm 0.2$	76.9 ± 5.5	6.0 ± 4.2	17.1 ± 5.0
$f_2'(1525)$	$10.7 \pm 0.7 \pm 0.9$	46.8 ± 1.9	33.8 ± 2.3	19.4 ± 2.3
$\phi(1680)$	$4.0 \pm 0.3 \pm 0.3$	44.0 ± 3.9	32.7 ± 3.6	23.3 ± 3.6
$f_2(1750)$	$0.59\,^{+0.23}_{-0.16} \pm 0.21$	58.2 ± 13.9	31.7 ± 12.4	$10.1\,^{+16.8}_{-6.1}$
$f_2(1950)$	$0.44\,^{+0.15}_{-0.10} \pm 0.14$	$2.2\,^{+6.7}_{-1.5}$	38.3 ± 13.8	59.5 ± 14.2
S-wave	$10.69 \pm 0.12 \pm 0.57$	100	0	0

Table 3. Fit results of the resonant structure.

over the same area, as given in eq. (8.4)

$$FF_i = \int |A_i|^2 \mathrm{d}m_{KK}\,\mathrm{d}\Omega / \int |\mathcal{A}|^2 \mathrm{d}m_{KK}\,\mathrm{d}\Omega. \tag{8.4}$$

The sum of the fit fractions is not necessarily unity due to the potential presence of interference between two resonances.

The fit fractions are reported in table 3 and resonance phases in table 4. Fit projections are shown in figure 6 for the $\phi(1020)$ region and above. The fit reproduces the data in each of the projected variables. Each contributing component is shown in figure 7 as a function of m_{KK}. To check the fit quality in the high m_{KK} region, χ^2 tests are performed. For m_{KK} and Ω, χ^2=1401 for 1125 bins (25 for m_{KK}, 5 for $\cos\theta_{KK}$, 3 for $\cos\theta_{J/\psi}$ and 3 for χ); for the two variables m_{KK} and $\cos\theta_{KK}$, χ^2=380 for 310 bins. The fit describes the data well. Note, adding the $f_2(1640)$ into the fit improves the $-2\ln\mathcal{L}$ by 0.4 with an additional 6 degrees of freedom, showing that this state is not observed.

As a check a fit is performed allowing independent sets of *CP*-violating parameters $(|\lambda_i|, \phi_s^i)$: three sets for the three corresponding $\phi(1020)$ transversity states, one for the K^+K^- S-wave, one common to all three transversity states of the $f_2(1270)$, one for the $f_2'(1525)$, one for the $\phi(1680)$, and one for the combination of the two high-mass $f_2(1750)$ and $f_2(1950)$ resonances. In total, eight sets of *CP*-violating parameters are used instead of two sets in the nominal fit. The $-2\ln\mathcal{L}$ value is improved by 16 units with 12 additional parameters compared to the nominal fit, corresponding to the fact that all states have consistent *CP* violation within $1.3\,\sigma$. All values of $|\lambda|$ are consistent with unity and ϕ_s differences of the longitudinal $\phi(1020)$ component are consistent with zero, showing no dependence of *CP* violation for the different states.

9 Systematic uncertainties

The systematic uncertainties are summarized for the physics parameters in table 5 and for the fit fractions in table 6. They are small compared to the statistical ones for the *CP*-violating parameters. Generally, the largest contribution results from the resonance

JHEP08(2017)037

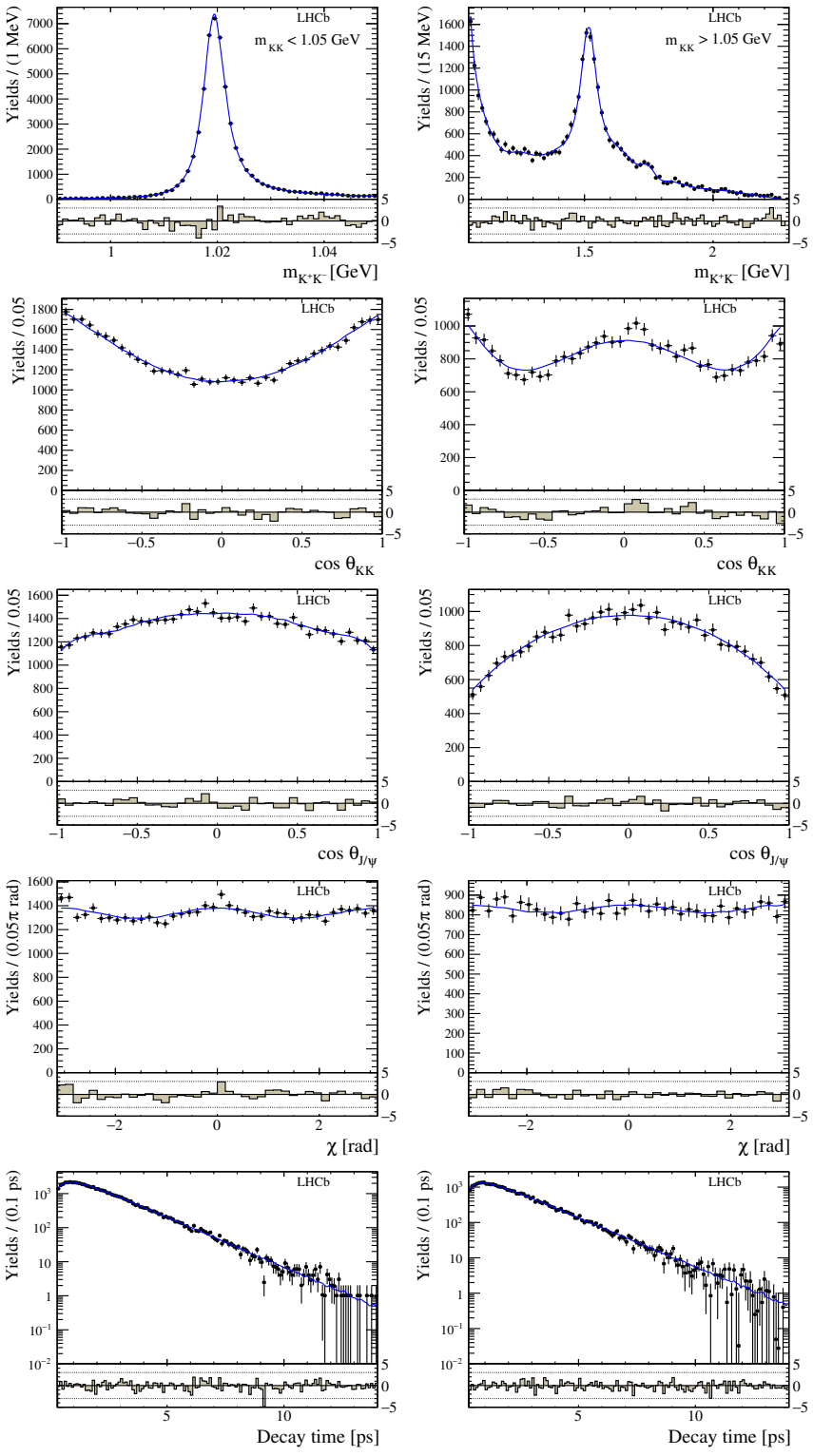

Figure 6. Projections of the fitting variables in the (left) low-mass ($\phi(1020)$) and (right) high-mass regions shown by the solid (blue) curves. The points with error bars are the data. At the bottom of each figure the differences between the data and the fit divided by the uncertainty in the data are shown.

JHEP08(2017)037

States	Phase difference (°)
$f_2(1270)^0 - \phi^\perp$	139.5 ± 6.5
$f_2'(1525)^0 - \phi^\perp$	-167.9 ± 6.6
$f_2(1750)^0 - \phi^\perp$	-251.5 ± 13.0
$f_2(1950)^0 - \phi^\perp$	-84.1 ± 42.1
$\phi(1680)^0 - \phi^0$	181.5 ± 5.2
$f_2(1270)^\perp - \phi^0$	100.5 ± 16.1
$f_2'(1525)^\perp - \phi^0$	-145.4 ± 9.2
$f_2(1750)^\perp - \phi^0$	230.2 ± 36.1
$f_2(1950)^\perp - \phi^0$	116.7 ± 17.4
$\phi^\perp - \phi^0$	199.7 ± 7.6
$\phi(1680)^\perp - \phi^\perp$	134.0 ± 7.6
$f_2(1270)^\parallel - \phi^\perp$	-140.3 ± 21.4
$f_2'(1525)^\parallel - \phi^\perp$	46.2 ± 7.9
$f_2(1750)^\parallel - \phi^\perp$	-27.5 ± 15.9
$f_2(1950)^\parallel - \phi^\perp$	3.8 ± 19.5
$\phi^\parallel - \phi^0$	195.4 ± 3.8
$\phi(1680)^\parallel - \phi^0$	-105.8 ± 8.9

Table 4. Fitted phase differences between two transversity states (statistical uncertainty only). Here the symbol ϕ refers to the components of the $\phi(1020)$ meson.

fit model. The fit model uncertainties are determined by doubling the number of S-wave knots in the high m_{KK} region, allowing the centrifugal barrier factors, of nominal value $1.5\,\mathrm{GeV}^{-1}$ for K^+K^- resonances and $5.0\,\mathrm{GeV}^{-1}$ for the B_s^0 meson [35], to vary within 0.5–2 times of these values [47]. Additional systematic uncertainties are evaluated by increasing the orbital angular momentum between the J/ψ and the K^+K^- system from the lowest allowed one, which is taken as the nominal value, and varying the masses and widths of contributing resonances by their uncertainties. The largest variation among those changes is assigned as the systematic uncertainty for resonance modelling. The effect of using the m_0 in the fit, rather than following the Belle approach using m_{KK} is evaluated by redoing the fit. This change worsens the $-2\ln\mathcal{L}$ by more than 100 units, which clearly shows the variation doesn't give a good fit; as a consequence, no systematic uncertainty is assessed. Differences resulting from the two conventions are comparable to the quoted modelling uncertainty for the *CP*-violating parameters, but generally are larger than the quoted systematic uncertainties for the fit fractions of nonscalar resonances.

The sources of uncertainty for the modelling of the efficiency variation of the three angles and m_{KK} include the statistical uncertainty from simulation, and the efficiency correction due to the differences in kinematic distributions between data and simulation

JHEP08(2017)037

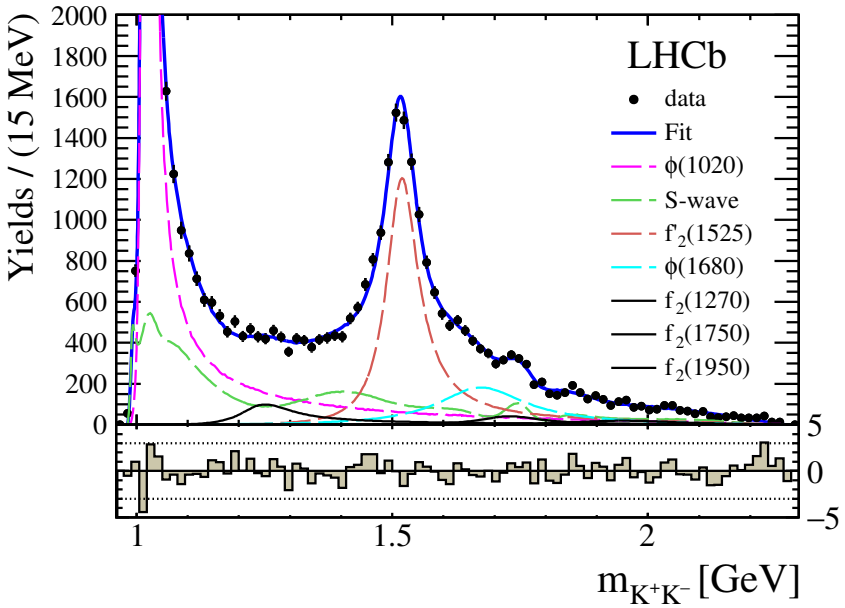

Figure 7. Fit projection of m_{KK}. The points represent the data; the resonances $\phi(1020)$, $f_2'(1525)$, $\phi(1680)$ are shown by magenta, brown, and cyan long-dashed curves, respectively; the S-wave component is depicted by green long-dashed curves; the other f_2 resonances are described by black solid curves; and the total fit by a blue solid curve. At the bottom the differences between the data and the fit divided by the uncertainty in the data are shown.

Source $\times 10^{-3}$	$\Delta\Gamma_s$ [ps^{-1}]	Γ_s [ps^{-1}]	$\lvert\lambda\rvert$	M_0 [GeV]	Γ_0 [GeV]	ϕ_s [rad]
Resonance modelling	6.9	1.9	5.5	1.1	3.6	23.6
Efficiency (m_{KK}, Ω)	3.0	0.9	0.5	0.1	0.7	3.4
Efficiency t	2.2	2.8	0.0	0.0	0.0	0.0
$\tau_{\overline{B}^0}$	1.4	2.0	0.0	0.0	0.0	0.0
t resolution	0.3	0.2	0.2	0.0	0.0	1.1
Fit bias	5.0	1.1	-	-	-	-
$A_{\rm P}$	0.1	0.3	1.4	0.0	0.0	4.0
Tagging	1.2	0.3	0.8	0.0	0.0	11.2
Background	0.5	0.8	0.4	0.1	0.1	1.5
sWeights	1.1	0.1	0.5	0.1	0.4	21.4
B_c^+	-	0.5	-	-	-	-
Total syst.	9.6	4.3	5.7	1.1	3.7	34.2
Stat.	17.7	5.5	18.0	1.3	3.0	106.6

Table 5. Absolute systematic uncertainties for the physics parameters determined from the high m_{KK} region compared to the corresponding statistical uncertainty. Here M_0 and Γ_0 refer to the uncertainties on the $f_2'(1525)$ resonance mass and width.

JHEP08(2017)037

Source	$\phi(1020)$	S-wave	$f_2'(1525)$	$\phi(1680)$	$f_2(1270)$	$f_2(1750)$	$f_2(1950)$
Res. modelling	0.99	0.57	0.73	0.27	0.21	0.21	0.13
Efficiency	0.58	0.06	0.48	0.12	0.04	0.03	0.01
Background	0.06	0.01	0.06	0.02	0.02	0.01	0.00
sWeights	0.11	0.02	0.16	0.05	0.02	0.05	0.04
Total syst.	1.15	0.57	0.89	0.30	0.21	0.21	0.14
Statistical	0.62	0.12	0.67	0.32	0.27	$^{+0.23}_{-0.16}$	$^{+0.15}_{-0.10}$

Table 6. Combined systematic and statistical uncertainties in the fit fractions using an absolute scale where the numbers are in units of %. "Res. modelling" refers to resonance modelling.

for B_s^0 decays. The former is estimated by repeating the fit to the data 100 times. In each fit, the efficiency parameters are resampled according to the corresponding covariance matrix determined from simulation. For the latter, the efficiency used by the nominal fit is obtained by weighting the distributions of p and $p_{\rm T}$ of the kaon pair and B_s^0 meson to match the data. Such weighting is removed to assign the corresponding systematic uncertainty.

The uncertainties due to the B^0 lifetime and decay time efficiency determination are estimated. Each source is evaluated by adding to the nominal fit an external correlated multidimensional Gaussian constraint, either given by the fit to the $\overline{B}^0 \to J/\psi\,\overline{K}^{*0}$ sample with varying $\tau_{B^0} = 1.520 \pm 0.004\,\text{ps}$ [24], or given by the fit to simulation for the decay time efficiency correction, i.e. $\varepsilon_{\rm sim}^{B_s^0}(t)/\varepsilon_{\rm sim}^{B^0}(t)$ in eq. (5.1). A systematic uncertainty is given by the difference in quadrature of the statistical uncertainties for each physics parameter between the nominal fit and the alternative fit with each of these constraints. The uncertainties due to the decay time acceptance are found to be negligible for the fit fraction results.

The sample of prompt J/ψ mesons combined with two kaon candidates is used to calibrate the per-candidate decay-time error. This method is validated by simulation. Since the detached selection, pointing angle and BDTG requirements cannot be applied to the calibration sample, the simulations show that the calibration overestimates the resolution for B_s^0 decays after final selection by about 4.5%. Therefore, a 5% variation of the widths, and the uncertainty of the mean value are used to estimate uncertainty of the time resolution modelling. The average angular resolution is 6 mrad for all three decay angles. This is small enough to have only negligible effects on the analysis.

A large number of pseudoexperiments is used to validate the fitter and check potential biases in the fit outputs. Biases on Γ_s and $\Delta\Gamma_s$, 20% of their statistical uncertainties, are taken as systematic uncertainties. Calibration parameters of the flavour-tagging algorithm and the B_s^0–$\overline{B}_s^0$ production asymmetry $A_{\rm P} = (1.09 \pm 2.69)\%$ [44] are fixed. The systematic uncertainties due to the calibration of the tagging parameters or the value of $A_{\rm P}$ are given by the difference in quadrature between the statistical uncertainty for each physics parameter between the nominal fit and an alternative fit where the tagging parameters or $A_{\rm P}$ are Gaussian-constrained by the corresponding uncertainties. Background sources are tested by varying the decay-time acceptance of the injected reflection backgrounds, changing these background yields by 5%, and also varying the Λ_b^0 lifetime.

JHEP08(2017)037

	Γ_s	$\Delta\Gamma_s$	ϕ_s	$\lvert\lambda\rvert$
Γ_s	+1.00	+0.54	+0.02	−0.03
$\Delta\Gamma_s$		+1.00	+0.04	−0.06
ϕ_s			+1.00	−0.14
$\lvert\lambda\rvert$				+1.00

Table 7. The correlation matrix from the high-mass region fit, taking into account both statistical and systematic uncertainties.

	Γ_s	$\Delta\Gamma_s$	ϕ_s	$\lvert\lambda\rvert$
Γ_s	+1.00	−0.13	−0.01	0.00
$\Delta\Gamma_s$		+1.00	−0.05	0.00
ϕ_s			+1.00	−0.04
$\lvert\lambda\rvert$				+1.00

Table 8. The correlation matrix taking into account both statistical and systematic uncertainties for the combination of the three measurements $B_s^0 \to J/\psi K^+K^-$ for $m_{KK} > 1.05\,\text{GeV}$, $m_{KK} < 1.05\,\text{GeV}$, and $J/\psi\pi^+\pi^-$.

To evaluate the uncertainty of the *sPlot* method that requires the fit observables being uncorrelated with the variable $m(J/\psi K^+K^-)$ used to obtain the *sWeights*, two variations are performed to obtain new *sWeights*, and the fit is repeated. The first consists of changing the number of $|\cos\theta_{J/\psi}|$ bins. In the nominal fit, the *sWeights* are determined by separate fits in four $|\cos\theta_{J/\psi}|$ bins for the event candidates, as significant variations of signal invariant mass resolution are seen as a function of the variable. In another variation of the analysis starting with the nominal number of $|\cos\theta_{J/\psi}|$ bins the decay time dependence is explored, since the combinatorial background may have a possible variation as a function of $m(J/\psi K^+K^-)$. Here the decay time is further divided into three intervals. The larger change on the physics parameter of interest is taken as a systematic uncertainty.

About 0.8% of the signal sample is expected from the decays of B_c^+ mesons [48]. Neglecting the B_c^+ contribution in the nominal fit leads to a negligible bias of $0.0005\,\text{ps}^{-1}$ for Γ_s [7]. The correlation matrix with both statistical and systematic uncertainties is shown in table 7.

10 Conclusions

We have studied B_s^0 and $\overline{B}_s^0$ decays into the $J/\psi K^+K^-$ final state using a time-dependent amplitude analysis. In the $m_{KK} > 1.05\,\text{GeV}$ region we determine

$$\begin{aligned}
\phi_s &= 119 \pm 107 \pm 34\,\text{mrad},\\
|\lambda| &= 0.994 \pm 0.018 \pm 0.006,\\
\Gamma_s &= 0.650 \pm 0.006 \pm 0.004\,\text{ps}^{-1},\\
\Delta\Gamma_s &= 0.066 \pm 0.018 \pm 0.010\,\text{ps}^{-1}.
\end{aligned}$$

JHEP08(2017)037

Many resonances and a S-wave structure have been found. Besides the $\phi(1020)$ meson these include the $f_2(1270)$, the $f_2'(1525)$, the $\phi(1680)$, the $f_2(1750)$, and the $f_2(1950)$ mesons. The presence of the $f_2(1640)$ resonance is not confirmed. The measured *CP*-violating parameters of the individual resonances are consistent. The $f_2'(1525)$ mass and width are determined as $1522.2 \pm 1.3 \pm 1.1\,\text{MeV}$ and $78.0 \pm 3.0 \pm 3.7\,\text{MeV}$, respectively. The fit fractions of the resonances in $B_s^0 \to J/\psi K^+K^-$ are also determined, and shown in table 3. These results supersede our previous measurements [14].

The combination with the previous results from B_s^0 decays in the $\phi(1020)$ region [7] gives

$$\begin{aligned}
\phi_s &= -25 \pm 45 \pm 8\,\text{mrad}, \\
|\lambda| &= 0.978 \pm 0.013 \pm 0.003, \\
\Gamma_s &= 0.6588 \pm 0.0022 \pm 0.0015\,\text{ps}^{-1}, \\
\Delta\Gamma_s &= 0.0813 \pm 0.0073 \pm 0.0036\,\text{ps}^{-1}.
\end{aligned}$$

The two results are consistent within 1.1σ. A further combination is performed by including the ϕ_s and $|\lambda|$ measurements from B_s^0 and $\overline{B}_s^0$ decays into $J/\psi\pi^+\pi^-$ [8], which results in $\phi_s = 1 \pm 37\,\text{mrad}$ and $|\lambda| = 0.973 \pm 0.013$, where Γ_s and $\Delta\Gamma_s$ are unchanged. The correlation matrix is shown in table 8. The measurement of the *CP*-violating phase ϕ_s is in agreement with the SM prediction $-36.5^{+1.3}_{-1.2}\,\text{mrad}$ [1]. These new combined results supersede our combination reported in ref. [7].

Acknowledgments

We express our gratitude to our colleagues in the CERN accelerator departments for the excellent performance of the LHC. We thank the technical and administrative staff at the LHCb institutes. We acknowledge support from CERN and from the national agencies: CAPES, CNPq, FAPERJ and FINEP (Brazil); MOST and NSFC (China); CNRS/IN2P3 (France); BMBF, DFG and MPG (Germany); INFN (Italy); NWO (The Netherlands); MNiSW and NCN (Poland); MEN/IFA (Romania); MinES and FASO (Russia); MinECo (Spain); SNSF and SER (Switzerland); NASU (Ukraine); STFC (United Kingdom); NSF (U.S.A.). We acknowledge the computing resources that are provided by CERN, IN2P3 (France), KIT and DESY (Germany), INFN (Italy), SURF (The Netherlands), PIC (Spain), GridPP (United Kingdom), RRCKI and Yandex LLC (Russia), CSCS (Switzerland), IFIN-HH (Romania), CBPF (Brazil), PL-GRID (Poland) and OSC (U.S.A.). We are indebted to the communities behind the multiple open source software packages on which we depend. Individual groups or members have received support from AvH Foundation (Germany), EPLANET, Marie Skłodowska-Curie Actions and ERC (European Union), Conseil Général de Haute-Savoie, Labex ENIGMASS and OCEVU, Région Auvergne (France), RFBR and Yandex LLC (Russia), GVA, XuntaGal and GENCAT (Spain), Herchel Smith Fund, The Royal Society, Royal Commission for the Exhibition of 1851 and the Leverhulme Trust (United Kingdom).

JHEP08(2017)037

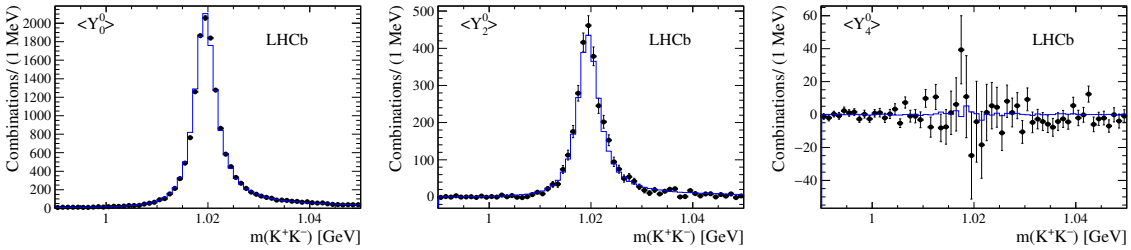

Figure 8. The K^+K^- mass dependence of the spherical harmonic moments of $\cos\theta_{KK}$ in the region of the $\phi(1020)$ resonance after efficiency corrections and background subtraction. The points with error bars are the data points and the (blue) lines are derived from the fit model.

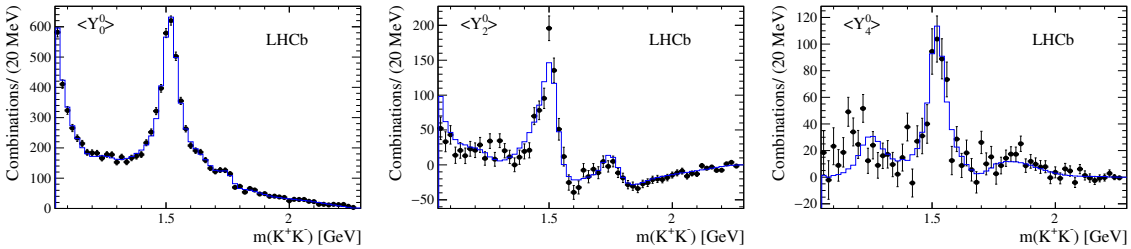

Figure 9. The K^+K^- mass dependence of the spherical harmonic moments of $\cos\theta_{KK}$ above the $\phi(1020)$ resonance region after efficiency corrections and background subtraction. The points with error bars are the data points and the (blue) lines are derived from the fit model.

A Angular moments

We define the moments $\langle Y_\ell^0 \rangle$, as the efficiency-corrected and background-subtracted K^+K^- invariant mass distributions, weighted by the ℓth spherical harmonic functions of the cosine of the helicity angle θ_{KK}. The moment distributions provide an additional way of visualizing the presence of different resonances and their interferences, similar to a partial wave analysis. Figures 8 and 9 show the distributions of the even angular moments for the events around ± 30 MeV of $\phi(1020)$ mass peak and those above the $\phi(1020)$, respectively. The general interpretation of the even moments is that $\langle Y_0^0 \rangle$ is the efficiency-corrected and background-subtracted event distribution, $\langle Y_2^0 \rangle$ reflects the sum of P-wave, D-wave and the interference of S-wave and D-wave amplitudes, and $\langle Y_4^0 \rangle$ the D-wave. The average of B_s^0 and $\overline{B}_s^0$ decays cancels the interference terms that involve P-wave amplitudes. This causes the odd moments to sum to zero.

The fit results reproduce the moment distributions relatively well. For the region near the $\phi(1020)$, the p-values are 3%, 3%, 48% for the ℓ=0, 2, 4 moments, respectively. For the high mass region, the p-values are 37%, 0.2% 0.5% for the ℓ=0, 2, 4 moments, respectively.

JHEP08(2017)037

References

[1] J. Charles et al., *Current status of the Standard Model CKM fit and constraints on $\Delta F = 2$ new physics*, *Phys. Rev.* **D 91** (2015) 073007 [arXiv:1501.05013] [INSPIRE].

[2] R. Fleischer, *Theoretical prospects for B physics*, PoS(FPCP2015)002 [arXiv:1509.00601] [INSPIRE].

[3] LHCb collaboration, *Measurement of the CP-violating phase β in $B^0 \to J/\psi\pi^+\pi^-$ decays and limits on penguin effects*, *Phys. Lett.* **B 742** (2015) 38 [arXiv:1411.1634] [INSPIRE].

[4] LHCb collaboration, *Measurement of CP-violation parameters and polarisation fractions in $B_s^0 \to J/\psi\overline{K}^{*0}$ decays*, *JHEP* **11** (2015) 082 [arXiv:1509.00400] [INSPIRE].

[5] D0 collaboration, V.M. Abazov et al., *Measurement of the CP-violating phase $\phi_s^{J/\psi\phi}$ using the flavor-tagged decay $B_s^0 \to J/\psi\phi$ in 8 fb^{-1} of $p\bar{p}$ collisions*, *Phys. Rev.* **D 85** (2012) 032006 [arXiv:1109.3166] [INSPIRE].

[6] CDF collaboration, T. Aaltonen et al., *Measurement of the bottom-strange meson mixing phase in the full CDF data set*, *Phys. Rev. Lett.* **109** (2012) 171802 [arXiv:1208.2967] [INSPIRE].

[7] LHCb collaboration, *Precision measurement of CP violation in $B_s^0 \to J/\psi K^+K^-$ decays*, *Phys. Rev. Lett.* **114** (2015) 041801 [arXiv:1411.3104] [INSPIRE].

[8] LHCb collaboration, *Measurement of the CP-violating phase ϕ_s in $\overline{B}_s^0 \to J/\psi\pi^+\pi^-$ decays*, *Phys. Lett.* **B 736** (2014) 186 [arXiv:1405.4140] [INSPIRE].

[9] CMS collaboration, *Measurement of the CP-violating weak phase ϕ_s and the decay width difference $\Delta\Gamma_s$ using the $B_s^0 \to J/\psi\phi(1020)$ decay channel in pp collisions at $\sqrt{s} = 8$ TeV*, *Phys. Lett.* **B 757** (2016) 97 [arXiv:1507.07527] [INSPIRE].

[10] ATLAS collaboration, *Measurement of the CP-violating phase ϕ_s and the B_s^0 meson decay width difference with $B_s^0 \to J/\psi\phi$ decays in ATLAS*, *JHEP* **08** (2016) 147 [arXiv:1601.03297] [INSPIRE].

[11] LHCb collaboration, *Measurement of the CP-violating phase ϕ_s in $\bar{B}_s^0 \to D_s^+D_s^-$ decays*, *Phys. Rev. Lett.* **113** (2014) 211801 [arXiv:1409.4619] [INSPIRE].

[12] LHCb collaboration, *First study of the CP-violating phase and decay-width difference in $B_s^0 \to \psi(2S)\phi$ decays*, *Phys. Lett.* **B 762** (2016) 253 [arXiv:1608.04855] [INSPIRE].

[13] Y. Amhis et al., *Averages of b-hadron, c-hadron and τ-lepton properties as of summer* 2016, arXiv:1612.07233 [INSPIRE].

[14] LHCb collaboration, *Amplitude analysis and the branching fraction measurement of $\bar{B}_s^0 \to J/\psi K^+K^-$*, *Phys. Rev.* **D 87** (2013) 072004 [arXiv:1302.1213] [INSPIRE].

[15] LHCb collaboration, *Observation of $B_s \to J/\psi f_2'(1525)$ in $J/\psi K^+K^-$ final states*, *Phys. Rev. Lett.* **108** (2012) 151801 [arXiv:1112.4695] [INSPIRE].

[16] L. Zhang and S. Stone, *Time-dependent Dalitz-plot formalism for $B_q \to J/\psi\ h^+h^-$*, *Phys. Lett.* **B 719** (2013) 383 [arXiv:1212.6434] [INSPIRE].

[17] A.S. Dighe, I. Dunietz, H.J. Lipkin and J.L. Rosner, *Angular distributions and lifetime differences in $B_s \to J/\psi\phi$ decays*, *Phys. Lett.* **B 369** (1996) 144 [hep-ph/9511363] [INSPIRE].

[18] I.I.Y. Bigi and A.I. Sanda, *CP violation*, *Camb. Monogr. Part. Phys. Nucl. Phys. Cosmol.* **9** (2000) 1 [INSPIRE].

JHEP08(2017)037

[19] LHCb collaboration, *Measurement of CP-violation and the B_s^0 meson decay width difference with $B_s^0 \to J/\psi K^+K^-$ and $B_s^0 \to J/\psi\pi^+\pi^-$ decays*, *Phys. Rev.* **D 87** (2013) 112010 [arXiv:1304.2600] [INSPIRE].

[20] LHCb collaboration, *Measurement of the CP asymmetry in B_s^0-$\overline{B}_s^0$ mixing*, *Phys. Rev. Lett.* **117** (2016) 061803 [*Addendum ibid.* **118** (2017) 129903] [arXiv:1605.09768] [INSPIRE].

[21] LHCb collaboration, *The LHCb detector at the LHC*, 2008 *JINST* **3** S08005 [INSPIRE].

[22] LHCb collaboration, *LHCb detector performance*, *Int. J. Mod. Phys.* **A 30** (2015) 1530022 [arXiv:1412.6352] [INSPIRE].

[23] P. Morawski and M. Witek, *Primary vertex reconstruction at LHCb*, LHCb-PUB-2014-044, CERN, Geneva Switzerland, (2014).

[24] Particle Data Group collaboration, C. Patrignani et al., *Review of particle physics*, *Chin. Phys.* **C 40** (2016) 100001 [INSPIRE].

[25] T. Sjöstrand, S. Mrenna and P.Z. Skands, *PYTHIA* 6.4 *physics and manual*, *JHEP* **05** (2006) 026 [hep-ph/0603175] [INSPIRE].

[26] T. Sjöstrand, S. Mrenna and P.Z. Skands, *A brief introduction to PYTHIA* 8.1, *Comput. Phys. Commun.* **178** (2008) 852 [arXiv:0710.3820] [INSPIRE].

[27] D.J. Lange, *The EvtGen particle decay simulation package*, *Nucl. Instrum. Meth.* **A 462** (2001) 152 [INSPIRE].

[28] P. Golonka and Z. Was, *PHOTOS Monte Carlo: a precision tool for QED corrections in Z and W decays*, *Eur. Phys. J.* **C 45** (2006) 97 [hep-ph/0506026] [INSPIRE].

[29] J. Allison et al., *GEANT4 developments and applications*, *IEEE Trans. Nucl. Sci.* **53** (2006) 270 [INSPIRE].

[30] GEANT4 collaboration, S. Agostinelli et al., *GEANT4: a simulation toolkit*, *Nucl. Instrum. Meth.* **A 506** (2003) 250 [INSPIRE].

[31] LHCb collaboration, *The LHCb simulation application, Gauss: design, evolution and experience*, *J. Phys. Conf. Ser.* **331** (2011) 032023 [INSPIRE].

[32] L. Breiman, J.H. Friedman, R.A. Olshen and C.J. Stone, *Classification and regression trees*, Wadsworth international group, Belmont CA U.S.A., (1984) [INSPIRE].

[33] M. Adinolfi et al., *Performance of the LHCb RICH detector at the LHC*, *Eur. Phys. J.* **C 73** (2013) 2431 [arXiv:1211.6759] [INSPIRE].

[34] Belle collaboration, K. Chilikin et al., *Observation of a new charged charmoniumlike state in $\bar{B}^0 \to J/\psi K^-\pi^+$ decays*, *Phys. Rev.* **D 90** (2014) 112009 [arXiv:1408.6457] [INSPIRE].

[35] LHCb collaboration, *Observation of $J/\psi p$ resonances consistent with pentaquark states in $\Lambda_b^0 \to J/\psi K^- p$ decays*, *Phys. Rev. Lett.* **115** (2015) 072001 [arXiv:1507.03414] [INSPIRE].

[36] D. Martínez Santos and F. Dupertuis, *Mass distributions marginalized over per-event errors*, *Nucl. Instrum. Meth.* **A 764** (2014) 150 [arXiv:1312.5000] [INSPIRE].

[37] LHCb collaboration, *Opposite-side flavour tagging of B mesons at the LHCb experiment*, *Eur. Phys. J.* **C 72** (2012) 2022 [arXiv:1202.4979] [INSPIRE].

[38] LHCb collaboration, *A new algorithm for identifying the flavour of B_s^0 mesons at LHCb*, 2016 *JINST* **11** P05010 [arXiv:1602.07252] [INSPIRE].

JHEP08(2017)037

[39] Belle collaboration, C.P. Shen et al., *Observation of the $\phi(1680)$ and the $Y(2175)$ in $e^+e^- \to \phi\pi^+\pi^-$*, *Phys. Rev.* **D 80** (2009) 031101 [arXiv:0808.0006] [INSPIRE].

[40] Belle collaboration, K. Abe et al., *Measurement of K^+K^- production in two photon collisions in the resonant mass region*, *Eur. Phys. J.* **C 32** (2003) 323 [hep-ex/0309077] [INSPIRE].

[41] Belle collaboration, R. Mizuk et al., *Observation of two resonance-like structures in the $\pi^+\chi_{c1}$ mass distribution in exclusive $\bar{B}^0 \to K^-\pi^+\chi_{c1}$ decays*, *Phys. Rev.* **D 78** (2008) 072004 [arXiv:0806.4098] [INSPIRE].

[42] M. Pivk and F.R. Le Diberder, *SPlot: a statistical tool to unfold data distributions*, *Nucl. Instrum. Meth.* **A 555** (2005) 356 [physics/0402083] [INSPIRE].

[43] Y. Xie, *sFit: a method for background subtraction in maximum likelihood fit*, arXiv:0905.0724 [INSPIRE].

[44] LHCb collaboration, *Measurement of the $\bar{B}^0$-B^0 and $\bar{B}^0_s$-B^0_s production asymmetries in pp collisions at $\sqrt{s} = 7$ TeV*, *Phys. Lett.* **B 739** (2014) 218 [arXiv:1408.0275] [INSPIRE].

[45] LHCb collaboration, *Measurement of B^0, B^0_s, B^+ and Λ^0_b production asymmetries in 7 and 8 TeV proton-proton collisions*, arXiv:1703.08464 [INSPIRE].

[46] LHCb collaboration, *Precision measurement of the B^0_s-$\bar{B}^0_s$ oscillation frequency with the decay $B^0_s \to D^-_s\pi^+$*, *New J. Phys.* **15** (2013) 053021 [arXiv:1304.4741] [INSPIRE].

[47] F. Von Hippel and C. Quigg, *Centrifugal-barrier effects in resonance partial decay widths, shapes and production amplitudes*, *Phys. Rev.* **D 5** (1972) 624 [INSPIRE].

[48] LHCb collaboration, *Observation of the decay $B^+_c \to B^0_s\pi^+$*, *Phys. Rev. Lett.* **111** (2013) 181801 [arXiv:1308.4544] [INSPIRE].

JHEP08(2017)037

The LHCb collaboration

R. Aaij[40], B. Adeva[39], M. Adinolfi[48], Z. Ajaltouni[5], S. Akar[59], J. Albrecht[10], F. Alessio[40], M. Alexander[53], S. Ali[43], G. Alkhazov[31], P. Alvarez Cartelle[55], A.A. Alves Jr[59], S. Amato[2], S. Amerio[23], Y. Amhis[7], L. An[3], L. Anderlini[18], G. Andreassi[41], M. Andreotti[17,g], J.E. Andrews[60], R.B. Appleby[56], F. Archilli[43], P. d'Argent[12], J. Arnau Romeu[6], A. Artamonov[37], M. Artuso[61], E. Aslanides[6], G. Auriemma[26], M. Baalouch[5], I. Babuschkin[56], S. Bachmann[12], J.J. Back[50], A. Badalov[38], C. Baesso[62], S. Baker[55], V. Balagura[7,c], W. Baldini[17], A. Baranov[35], R.J. Barlow[56], C. Barschel[40], S. Barsuk[7], W. Barter[56], F. Baryshnikov[32], M. Baszczyk[27,l], V. Batozskaya[29], B. Batsukh[61], V. Battista[41], A. Bay[41], L. Beaucourt[4], J. Beddow[53], F. Bedeschi[24], I. Bediaga[1], A. Beiter[61], L.J. Bel[43], V. Bellee[41], N. Belloli[21,i], K. Belous[37], I. Belyaev[32], E. Ben-Haim[8], G. Bencivenni[19], S. Benson[43], S. Beranek[9], A. Berezhnoy[33], R. Bernet[42], A. Bertolin[23], C. Betancourt[42], F. Betti[15], M.-O. Bettler[40], M. van Beuzekom[43], Ia. Bezshyiko[42], S. Bifani[47], P. Billoir[8], A. Birnkraut[10], A. Bitadze[56], A. Bizzeti[18,u], T. Blake[50], F. Blanc[41], J. Blouw[11,†], S. Blusk[61], V. Bocci[26], T. Boettcher[58], A. Bondar[36,w], N. Bondar[31], W. Bonivento[16], I. Bordyuzhin[32], A. Borgheresi[21,i], S. Borghi[56], M. Borisyak[35], M. Borsato[39], F. Bossu[7], M. Boubdir[9], T.J.V. Bowcock[54], E. Bowen[42], C. Bozzi[17,40], S. Braun[12], T. Britton[61], J. Brodzicka[56], E. Buchanan[48], C. Burr[56], A. Bursche[2], J. Buytaert[40], S. Cadeddu[16], R. Calabrese[17,g], M. Calvi[21,i], M. Calvo Gomez[38,m], A. Camboni[38], P. Campana[19], D.H. Campora Perez[40], L. Capriotti[56], A. Carbone[15,e], G. Carboni[25,j], R. Cardinale[20,h], A. Cardini[16], P. Carniti[21,i], L. Carson[52], K. Carvalho Akiba[2], G. Casse[54], L. Cassina[21,i], L. Castillo Garcia[41], M. Cattaneo[40], G. Cavallero[20], R. Cenci[24,t], D. Chamont[7], M. Charles[8], Ph. Charpentier[40], G. Chatzikonstantinidis[47], M. Chefdeville[4], S. Chen[56], S.F. Cheung[57], V. Chobanova[39], M. Chrzaszcz[42,27], A. Chubykin[31], X. Cid Vidal[39], G. Ciezarek[43], P.E.L. Clarke[52], M. Clemencic[40], H.V. Cliff[49], J. Closier[40], V. Coco[59], J. Cogan[6], E. Cogneras[5], V. Cogoni[16,f], L. Cojocariu[30], P. Collins[40], A. Comerma-Montells[12], A. Contu[40], A. Cook[48], G. Coombs[40], S. Coquereau[38], G. Corti[40], M. Corvo[17,g], C.M. Costa Sobral[50], B. Couturier[40], G.A. Cowan[52], D.C. Craik[52], A. Crocombe[50], M. Cruz Torres[62], S. Cunliffe[55], R. Currie[52], C. D'Ambrosio[40], F. Da Cunha Marinho[2], E. Dall'Occo[43], J. Dalseno[48], A. Davis[3], K. De Bruyn[6], S. De Capua[56], M. De Cian[12], J.M. De Miranda[1], L. De Paula[2], M. De Serio[14,d], P. De Simone[19], C.T. Dean[53], D. Decamp[4], M. Deckenhoff[10], L. Del Buono[8], H.-P. Dembinski[11], M. Demmer[10], A. Dendek[28], D. Derkach[35], O. Deschamps[5], F. Dettori[54], B. Dey[22], A. Di Canto[40], P. Di Nezza[19], H. Dijkstra[40], F. Dordei[40], M. Dorigo[41], A. Dosil Suárez[39], A. Dovbnya[45], K. Dreimanis[54], L. Dufour[43], G. Dujany[56], K. Dungs[40], P. Durante[40], R. Dzhelyadin[37], M. Dziewiecki[12], A. Dziurda[40], A. Dzyuba[31], N. Déléage[4], S. Easo[51], M. Ebert[52], U. Egede[55], V. Egorychev[32], S. Eidelman[36,w], S. Eisenhardt[52], U. Eitschberger[10], R. Ekelhof[10], L. Eklund[53], S. Ely[61], S. Esen[12], H.M. Evans[49], T. Evans[57], A. Falabella[15], N. Farley[47], S. Farry[54], R. Fay[54], D. Fazzini[21,i], D. Ferguson[52], G. Fernandez[38], A. Fernandez Prieto[39], F. Ferrari[15], F. Ferreira Rodrigues[2], M. Ferro-Luzzi[40], S. Filippov[34], R.A. Fini[14], M. Fiore[17,g], M. Fiorini[17,g], M. Firlej[28], C. Fitzpatrick[41], T. Fiutowski[28], F. Fleuret[7,b], K. Fohl[40], M. Fontana[16,40], F. Fontanelli[20,h], D.C. Forshaw[61], R. Forty[40], V. Franco Lima[54], M. Frank[40], C. Frei[40], J. Fu[22,q], W. Funk[40], E. Furfaro[25,j], C. Färber[40], A. Gallas Torreira[39], D. Galli[15,e], S. Gallorini[23], S. Gambetta[52], M. Gandelman[2], P. Gandini[57], Y. Gao[3], L.M. Garcia Martin[69], J. García Pardiñas[39], J. Garra Tico[49], L. Garrido[38], P.J. Garsed[49], D. Gascon[38], C. Gaspar[40], L. Gavardi[10], G. Gazzoni[5], D. Gerick[12], E. Gersabeck[12], M. Gersabeck[56], T. Gershon[50], Ph. Ghez[4], S. Gianì[41], V. Gibson[49], O.G. Girard[41], L. Giubega[30], K. Gizdov[52], V.V. Gligorov[8], D. Golubkov[32], A. Golutvin[55,40], A. Gomes[1,a], I.V. Gorelov[33], C. Gotti[21,i], E. Govorkova[43], R. Graciani Diaz[38], L.A. Granado Cardoso[40], E. Graugés[38], E. Graverini[42], G. Graziani[18],

JHEP08(2017)037

A. Grecu[30], R. Greim[9], P. Griffith[16], L. Grillo[21,40,i], B.R. Gruberg Cazon[57], O. Grünberg[67], E. Gushchin[34], Yu. Guz[37], T. Gys[40], C. Göbel[62], T. Hadavizadeh[57], C. Hadjivasiliou[5], G. Haefeli[41], C. Haen[40], S.C. Haines[49], B. Hamilton[60], X. Han[12], S. Hansmann-Menzemer[12], N. Harnew[57], S.T. Harnew[48], J. Harrison[56], M. Hatch[40], J. He[63], T. Head[41], A. Heister[9], K. Hennessy[54], P. Henrard[5], L. Henry[69], E. van Herwijnen[40], M. Heß[67], A. Hicheur[2], D. Hill[57], C. Hombach[56], P.H. Hopchev[41], Z.-C. Huard[59], W. Hulsbergen[43], T. Humair[55], M. Hushchyn[35], D. Hutchcroft[54], M. Idzik[28], P. Ilten[58], R. Jacobsson[40], J. Jalocha[57], E. Jans[43], A. Jawahery[60], F. Jiang[3], M. John[57], D. Johnson[40], C.R. Jones[49], C. Joram[40], B. Jost[40], N. Jurik[57], S. Kandybei[45], M. Karacson[40], J.M. Kariuki[48], S. Karodia[53], M. Kecke[12], M. Kelsey[61], M. Kenzie[49], T. Ketel[44], E. Khairullin[35], B. Khanji[12], C. Khurewathanakul[41], T. Kirn[9], S. Klaver[56], K. Klimaszewski[29], T. Klimkovich[11], S. Koliiev[46], M. Kolpin[12], I. Komarov[41], R. Kopecna[12], P. Koppenburg[43], A. Kosmyntseva[32], S. Kotriakhova[31], A. Kozachuk[33], M. Kozeiha[5], L. Kravchuk[34], M. Kreps[50], P. Krokovny[36,w], F. Kruse[10], W. Krzemien[29], W. Kucewicz[27,l], M. Kucharczyk[27], V. Kudryavtsev[36,w], A.K. Kuonen[41], K. Kurek[29], T. Kvaratskheliya[32,40], D. Lacarrere[40], G. Lafferty[56], A. Lai[16], G. Lanfranchi[19], C. Langenbruch[9], T. Latham[50], C. Lazzeroni[47], R. Le Gac[6], J. van Leerdam[43], A. Leflat[33,40], J. Lefrançois[7], R. Lefèvre[5], F. Lemaitre[40], E. Lemos Cid[39], O. Leroy[6], T. Lesiak[27], B. Leverington[12], T. Li[3], Y. Li[7], Z. Li[61], T. Likhomanenko[35,68], R. Lindner[40], F. Lionetto[42], X. Liu[3], D. Loh[50], I. Longstaff[53], J.H. Lopes[2], D. Lucchesi[23,o], M. Lucio Martinez[39], H. Luo[52], A. Lupato[23], E. Luppi[17,g], O. Lupton[40], A. Lusiani[24], X. Lyu[63], F. Machefert[7], F. Maciuc[30], O. Maev[31], K. Maguire[56], S. Malde[57], A. Malinin[68], T. Maltsev[36], G. Manca[16,f], G. Mancinelli[6], P. Manning[61], J. Maratas[5,v], J.F. Marchand[4], U. Marconi[15], C. Marin Benito[38], M. Marinangeli[41], P. Marino[24,t], J. Marks[12], G. Martellotti[26], M. Martin[6], M. Martinelli[41], D. Martinez Santos[39], F. Martinez Vidal[69], D. Martins Tostes[2], L.M. Massacrier[7], A. Massafferri[1], R. Matev[40], A. Mathad[50], Z. Mathe[40], C. Matteuzzi[21], A. Mauri[42], E. Maurice[7,b], B. Maurin[41], A. Mazurov[47], M. McCann[55,40], A. McNab[56], R. McNulty[13], B. Meadows[59], F. Meier[10], D. Melnychuk[29], M. Merk[43], A. Merli[22,40,q], E. Michielin[23], D.A. Milanes[66], M.-N. Minard[4], D.S. Mitzel[12], A. Mogini[8], J. Molina Rodriguez[1], I.A. Monroy[66], S. Monteil[5], M. Morandin[23], M.J. Morello[24,t], O. Morgunova[68], J. Moron[28], A.B. Morris[52], R. Mountain[61], F. Muheim[52], M. Mulder[43], M. Mussini[15], D. Müller[56], J. Müller[10], K. Müller[42], V. Müller[10], P. Naik[48], T. Nakada[41], R. Nandakumar[51], A. Nandi[57], I. Nasteva[2], M. Needham[52], N. Neri[22,40], S. Neubert[12], N. Neufeld[40], M. Neuner[12], T.D. Nguyen[41], C. Nguyen-Mau[41,n], S. Nieswand[9], R. Niet[10], N. Nikitin[33], T. Nikodem[12], A. Nogay[68], A. Novoselov[37], D.P. O'Hanlon[50], A. Oblakowska-Mucha[28], V. Obraztsov[37], S. Ogilvy[19], R. Oldeman[16,f], C.J.G. Onderwater[70], A. Ossowska[27], J.M. Otalora Goicochea[2], P. Owen[42], A. Oyanguren[69], P.R. Pais[41], A. Palano[14,d], M. Palutan[19,40], A. Papanestis[51], M. Pappagallo[14,d], L.L. Pappalardo[17,g], C. Pappenheimer[59], W. Parker[60], C. Parkes[56], G. Passaleva[18], A. Pastore[14,d], M. Patel[55], C. Patrignani[15,e], A. Pearce[40], A. Pellegrino[43], G. Penso[26], M. Pepe Altarelli[40], S. Perazzini[40], P. Perret[5], L. Pescatore[41], K. Petridis[48], A. Petrolini[20,h], A. Petrov[68], M. Petruzzo[22,q], E. Picatoste Olloqui[38], B. Pietrzyk[4], M. Pikies[27], D. Pinci[26], A. Pistone[20], A. Piucci[12], V. Placinta[30], S. Playfer[52], M. Plo Casasus[39], T. Poikela[40], F. Polci[8], M. Poli Lener[19], A. Poluektov[50,36], I. Polyakov[61], E. Polycarpo[2], G.J. Pomery[48], S. Ponce[40], A. Popov[37], D. Popov[11,40], B. Popovici[30], S. Poslavskii[37], C. Potterat[2], E. Price[48], J. Prisciandaro[39], C. Prouve[48], V. Pugatch[46], A. Puig Navarro[42], G. Punzi[24,p], C. Qian[63], W. Qian[50], R. Quagliani[7,48], B. Rachwal[28], J.H. Rademacker[48], M. Rama[24], M. Ramos Pernas[39], M.S. Rangel[2], I. Raniuk[45,†], F. Ratnikov[35], G. Raven[44], F. Redi[55], S. Reichert[10], A.C. dos Reis[1], C. Remon Alepuz[69], V. Renaudin[7], S. Ricciardi[51], S. Richards[48], M. Rihl[40], K. Rinnert[54], V. Rives Molina[38], P. Robbe[7], A.B. Rodrigues[1], E. Rodrigues[59], J.A. Rodriguez Lopez[66],

JHEP08(2017)037

P. Rodriguez Perez[56,†], A. Rogozhnikov[35], S. Roiser[40], A. Rollings[57], V. Romanovskiy[37], A. Romero Vidal[39], J.W. Ronayne[13], M. Rotondo[19], M.S. Rudolph[61], T. Ruf[40], P. Ruiz Valls[69], J.J. Saborido Silva[39], E. Sadykhov[32], N. Sagidova[31], B. Saitta[16,f], V. Salustino Guimaraes[1], D. Sanchez Gonzalo[38], C. Sanchez Mayordomo[69], B. Sanmartin Sedes[39], R. Santacesaria[26], C. Santamarina Rios[39], M. Santimaria[19], E. Santovetti[25,j], A. Sarti[19,k], C. Satriano[26,s], A. Satta[25], D.M. Saunders[48], D. Savrina[32,33], S. Schael[9], M. Schellenberg[10], M. Schiller[53], H. Schindler[40], M. Schlupp[10], M. Schmelling[11], T. Schmelzer[10], B. Schmidt[40], O. Schneider[41], A. Schopper[40], H.F. Schreiner[59], K. Schubert[10], M. Schubiger[41], M.-H. Schune[7], R. Schwemmer[40], B. Sciascia[19], A. Sciubba[26,k], A. Semennikov[32], A. Sergi[47], N. Serra[42], J. Serrano[6], L. Sestini[23], P. Seyfert[21], M. Shapkin[37], I. Shapoval[45], Y. Shcheglov[31], T. Shears[54], L. Shekhtman[36,w], V. Shevchenko[68], B.G. Siddi[17,40], R. Silva Coutinho[42], L. Silva de Oliveira[2], G. Simi[23,o], S. Simone[14,d], M. Sirendi[49], N. Skidmore[48], T. Skwarnicki[61], E. Smith[55], I.T. Smith[52], J. Smith[49], M. Smith[55], l. Soares Lavra[1], M.D. Sokoloff[59], F.J.P. Soler[53], B. Souza De Paula[2], B. Spaan[10], P. Spradlin[53], S. Sridharan[40], F. Stagni[40], M. Stahl[12], S. Stahl[40], P. Stefko[41], S. Stefkova[55], O. Steinkamp[42], S. Stemmle[12], O. Stenyakin[37], H. Stevens[10], S. Stoica[30], S. Stone[61], B. Storaci[42], S. Stracka[24,p], M.E. Stramaglia[41], M. Straticiuc[30], U. Straumann[42], L. Sun[64], W. Sutcliffe[55], K. Swientek[28], V. Syropoulos[44], M. Szczekowski[29], T. Szumlak[28], S. T'Jampens[4], A. Tayduganov[6], T. Tekampe[10], G. Tellarini[17,g], F. Teubert[40], E. Thomas[40], J. van Tilburg[43], M.J. Tilley[55], V. Tisserand[4], M. Tobin[41], S. Tolk[49], L. Tomassetti[17,g], D. Tonelli[24], S. Topp-Joergensen[57], F. Toriello[61], R. Tourinho Jadallah Aoude[1], E. Tournefier[4], S. Tourneur[41], K. Trabelsi[41], M. Traill[53], M.T. Tran[41], M. Tresch[42], A. Trisovic[40], A. Tsaregorodtsev[6], P. Tsopelas[43], A. Tully[49], N. Tuning[43], A. Ukleja[29], A. Ustyuzhanin[35], U. Uwer[12], C. Vacca[16,f], V. Vagnoni[15,40], A. Valassi[40], S. Valat[40], G. Valenti[15], R. Vazquez Gomez[19], P. Vazquez Regueiro[39], S. Vecchi[17], M. van Veghel[43], J.J. Velthuis[48], M. Veltri[18,r], G. Veneziano[57], A. Venkateswaran[61], T.A. Verlage[9], M. Vernet[5], M. Vesterinen[12], J.V. Viana Barbosa[40], B. Viaud[7], D. Vieira[63], M. Vieites Diaz[39], H. Viemann[67], X. Vilasis-Cardona[38,m], M. Vitti[49], V. Volkov[33], A. Vollhardt[42], B. Voneki[40], A. Vorobyev[31], V. Vorobyev[36,w], C. Voß[9], J.A. de Vries[43], C. Vázquez Sierra[39], R. Waldi[67], C. Wallace[50], R. Wallace[13], J. Walsh[24], J. Wang[61], D.R. Ward[49], H.M. Wark[54], N.K. Watson[47], D. Websdale[55], A. Weiden[42], M. Whitehead[40], J. Wicht[50], G. Wilkinson[57,40], M. Wilkinson[61], M. Williams[40], M.P. Williams[47], M. Williams[58], T. Williams[47], F.F. Wilson[51], J. Wimberley[60], M.A. Winn[7], J. Wishahi[10], W. Wislicki[29], M. Witek[27], G. Wormser[7], S.A. Wotton[49], K. Wraight[53], K. Wyllie[40], Y. Xie[65], Z. Xing[61], Z. Xu[4], Z. Yang[3], Z. Yang[60], Y. Yao[61], H. Yin[65], J. Yu[65], X. Yuan[61], O. Yushchenko[37], K.A. Zarebski[47], M. Zavertyaev[11,c], L. Zhang[3], Y. Zhang[7], A. Zhelezov[12], Y. Zheng[63], X. Zhu[3], V. Zhukov[33] and S. Zucchelli[15]

[1] *Centro Brasileiro de Pesquisas Físicas (CBPF), Rio de Janeiro, Brazil*
[2] *Universidade Federal do Rio de Janeiro (UFRJ), Rio de Janeiro, Brazil*
[3] *Center for High Energy Physics, Tsinghua University, Beijing, China*
[4] *LAPP, Université Savoie Mont-Blanc, CNRS/IN2P3, Annecy-Le-Vieux, France*
[5] *Clermont Université, Université Blaise Pascal, CNRS/IN2P3, LPC, Clermont-Ferrand, France*
[6] *CPPM, Aix-Marseille Université, CNRS/IN2P3, Marseille, France*
[7] *LAL, Université Paris-Sud, CNRS/IN2P3, Orsay, France*
[8] *LPNHE, Université Pierre et Marie Curie, Université Paris Diderot, CNRS/IN2P3, Paris, France*
[9] *I. Physikalisches Institut, RWTH Aachen University, Aachen, Germany*
[10] *Fakultät Physik, Technische Universität Dortmund, Dortmund, Germany*
[11] *Max-Planck-Institut für Kernphysik (MPIK), Heidelberg, Germany*
[12] *Physikalisches Institut, Ruprecht-Karls-Universität Heidelberg, Heidelberg, Germany*
[13] *School of Physics, University College Dublin, Dublin, Ireland*

JHEP08(2017)037

[14] *Sezione INFN di Bari, Bari, Italy*
[15] *Sezione INFN di Bologna, Bologna, Italy*
[16] *Sezione INFN di Cagliari, Cagliari, Italy*
[17] *Sezione INFN di Ferrara, Ferrara, Italy*
[18] *Sezione INFN di Firenze, Firenze, Italy*
[19] *Laboratori Nazionali dell'INFN di Frascati, Frascati, Italy*
[20] *Sezione INFN di Genova, Genova, Italy*
[21] *Sezione INFN di Milano Bicocca, Milano, Italy*
[22] *Sezione INFN di Milano, Milano, Italy*
[23] *Sezione INFN di Padova, Padova, Italy*
[24] *Sezione INFN di Pisa, Pisa, Italy*
[25] *Sezione INFN di Roma Tor Vergata, Roma, Italy*
[26] *Sezione INFN di Roma La Sapienza, Roma, Italy*
[27] *Henryk Niewodniczanski Institute of Nuclear Physics Polish Academy of Sciences, Kraków, Poland*
[28] *AGH - University of Science and Technology, Faculty of Physics and Applied Computer Science, Kraków, Poland*
[29] *National Center for Nuclear Research (NCBJ), Warsaw, Poland*
[30] *Horia Hulubei National Institute of Physics and Nuclear Engineering, Bucharest-Magurele, Romania*
[31] *Petersburg Nuclear Physics Institute (PNPI), Gatchina, Russia*
[32] *Institute of Theoretical and Experimental Physics (ITEP), Moscow, Russia*
[33] *Institute of Nuclear Physics, Moscow State University (SINP MSU), Moscow, Russia*
[34] *Institute for Nuclear Research of the Russian Academy of Sciences (INR RAN), Moscow, Russia*
[35] *Yandex School of Data Analysis, Moscow, Russia*
[36] *Budker Institute of Nuclear Physics (SB RAS), Novosibirsk, Russia*
[37] *Institute for High Energy Physics (IHEP), Protvino, Russia*
[38] *ICCUB, Universitat de Barcelona, Barcelona, Spain*
[39] *Universidad de Santiago de Compostela, Santiago de Compostela, Spain*
[40] *European Organization for Nuclear Research (CERN), Geneva, Switzerland*
[41] *Institute of Physics, Ecole Polytechnique Fédérale de Lausanne (EPFL), Lausanne, Switzerland*
[42] *Physik-Institut, Universität Zürich, Zürich, Switzerland*
[43] *Nikhef National Institute for Subatomic Physics, Amsterdam, The Netherlands*
[44] *Nikhef National Institute for Subatomic Physics and VU University Amsterdam, Amsterdam, The Netherlands*
[45] *NSC Kharkiv Institute of Physics and Technology (NSC KIPT), Kharkiv, Ukraine*
[46] *Institute for Nuclear Research of the National Academy of Sciences (KINR), Kyiv, Ukraine*
[47] *University of Birmingham, Birmingham, United Kingdom*
[48] *H.H. Wills Physics Laboratory, University of Bristol, Bristol, United Kingdom*
[49] *Cavendish Laboratory, University of Cambridge, Cambridge, United Kingdom*
[50] *Department of Physics, University of Warwick, Coventry, United Kingdom*
[51] *STFC Rutherford Appleton Laboratory, Didcot, United Kingdom*
[52] *School of Physics and Astronomy, University of Edinburgh, Edinburgh, United Kingdom*
[53] *School of Physics and Astronomy, University of Glasgow, Glasgow, United Kingdom*
[54] *Oliver Lodge Laboratory, University of Liverpool, Liverpool, United Kingdom*
[55] *Imperial College London, London, United Kingdom*
[56] *School of Physics and Astronomy, University of Manchester, Manchester, United Kingdom*
[57] *Department of Physics, University of Oxford, Oxford, United Kingdom*
[58] *Massachusetts Institute of Technology, Cambridge, MA, United States*
[59] *University of Cincinnati, Cincinnati, OH, United States*
[60] *University of Maryland, College Park, MD, United States*
[61] *Syracuse University, Syracuse, NY, United States*
[62] *Pontifícia Universidade Católica do Rio de Janeiro (PUC-Rio), Rio de Janeiro, Brazil, associated to* [2]

JHEP08(2017)037

[63] University of Chinese Academy of Sciences, Beijing, China, associated to [3]
[64] School of Physics and Technology, Wuhan University, Wuhan, China, associated to [3]
[65] Institute of Particle Physics, Central China Normal University, Wuhan, Hubei, China, associated to [3]
[66] Departamento de Fisica , Universidad Nacional de Colombia, Bogota, Colombia, associated to [8]
[67] Institut für Physik, Universität Rostock, Rostock, Germany, associated to [12]
[68] National Research Centre Kurchatov Institute, Moscow, Russia, associated to [32]
[69] Instituto de Fisica Corpuscular, Centro Mixto Universidad de Valencia - CSIC, Valencia, Spain, associated to [38]
[70] Van Swinderen Institute, University of Groningen, Groningen, The Netherlands, associated to [43]

[a] Universidade Federal do Triângulo Mineiro (UFTM), Uberaba-MG, Brazil
[b] Laboratoire Leprince-Ringuet, Palaiseau, France
[c] P.N. Lebedev Physical Institute, Russian Academy of Science (LPI RAS), Moscow, Russia
[d] Università di Bari, Bari, Italy
[e] Università di Bologna, Bologna, Italy
[f] Università di Cagliari, Cagliari, Italy
[g] Università di Ferrara, Ferrara, Italy
[h] Università di Genova, Genova, Italy
[i] Università di Milano Bicocca, Milano, Italy
[j] Università di Roma Tor Vergata, Roma, Italy
[k] Università di Roma La Sapienza, Roma, Italy
[l] AGH - University of Science and Technology, Faculty of Computer Science, Electronics and Telecommunications, Kraków, Poland
[m] LIFAELS, La Salle, Universitat Ramon Llull, Barcelona, Spain
[n] Hanoi University of Science, Hanoi, Viet Nam
[o] Università di Padova, Padova, Italy
[p] Università di Pisa, Pisa, Italy
[q] Università degli Studi di Milano, Milano, Italy
[r] Università di Urbino, Urbino, Italy
[s] Università della Basilicata, Potenza, Italy
[t] Scuola Normale Superiore, Pisa, Italy
[u] Università di Modena e Reggio Emilia, Modena, Italy
[v] Iligan Institute of Technology (IIT), Iligan, Philippines
[w] Novosibirsk State University, Novosibirsk, Russia
[†] Deceased

JHEP08(2017)037